© 2020. Published by The Company of Biologists Ltd | Journal of Cell Science (2020) 133, jcs247155. doi:10.1242/jcs.247155

RESEARCH ARTICLE

Staufen1 localizes to the mitotic spindle and controls the localization of RNA populations to the spindle

Sami Hassine[1,*], Florence Bonnet-Magnaval[1,*], Louis Philip Benoit Bouvrette[1,2], Bellastrid Doran[1], Mehdi Ghram[1], Mathieu Bouthillette[1], Eric Lecuyer[1,2] and Luc DesGroseillers[1,‡]

ABSTRACT

Staufen1 (STAU1) is an RNA-binding protein involved in the post-transcriptional regulation of mRNAs. We report that a large fraction of STAU1 localizes to the mitotic spindle in colorectal cancer HCT116 cells and in non-transformed hTERT-RPE1 cells. Spindle-associated STAU1 partly co-localizes with ribosomes and active sites of translation. We mapped the molecular determinant required for STAU1–spindle association within the first 88 N-terminal amino acids, a domain that is not required for RNA binding. Interestingly, transcriptomic analysis of purified mitotic spindles revealed that 1054 mRNAs and the precursor ribosomal RNA (pre-rRNA), as well as the long non-coding RNAs and small nucleolar RNAs involved in ribonucleoprotein assembly and processing, are enriched on spindles compared with cell extracts. STAU1 knockout causes displacement of the pre-rRNA and of 154 mRNAs coding for proteins involved in actin cytoskeleton organization and cell growth, highlighting a role for STAU1 in mRNA trafficking to spindle. These data demonstrate that STAU1 controls the localization of subpopulations of RNAs during mitosis and suggests a novel role of STAU1 in pre-rRNA maintenance during mitosis, ribogenesis and/or nucleoli reassembly.

KEY WORDS: Staufen1, RNA, Localization, Post-transcriptional regulation, Mitotic spindle, RNA-Seq, Ribosomal RNA

INTRODUCTION

The localization of RNA molecules to specific subcellular compartments, a cellular mechanism that is crucial for normal progression of several biological processes, functions to spatiotemporally regulate gene expression (Neriec and Percipalle, 2018; Suter, 2018; Mayya and Duchaine, 2019). Coordination of this post-transcriptional mechanism is controlled by RNA-binding proteins that are thought to bind and regulate overlapping groups of functionally related RNAs (Keene, 2007; Van Nostrand et al., 2020). This mechanism could allow subpopulations of mRNAs to be tagged and functionally grouped into RNA regulons, and ensure that proteins involved in a specific pathway are translated in a highly coordinated fashion.

Staufen1 (STAU1) is a double-stranded RNA binding protein well known for its involvement in the post-transcriptional regulation of gene expression (Wickham et al., 1999; Marion et al., 1999). It is ubiquitously expressed in mammals as alternatively spliced transcripts that generate protein isoforms of 55 kDa (STAU1^{55}, STAU1^{55i}) and 63 kDa (STAU1^{63}) (Wickham et al., 1999; Marion et al., 1999; Duchaine et al., 2000). A large fraction of STAU1-bound mRNAs are associated with translating ribosomes (Ricci et al., 2014; de Lucas et al., 2014; Luo et al., 2002). Genome-wide analyses reveal that STAU1-bound mRNAs code for proteins with heterogeneous functions including transcription, translation, cell growth and regulation of the cell cycle (Ricci et al., 2014; de Lucas et al., 2014; Furic et al., 2008; Laver et al., 2013; LeGendre et al., 2013; Sugimoto et al., 2015). Through its binding to specific mRNA populations, STAU1 controls RNA splicing (Ravel-Chapuis et al., 2012), nuclear export (Elbarbary et al., 2013; Ravel-Chapuis et al., 2012), transport and localization (Kiebler et al., 1999; Vessey et al., 2008), translation (Ricci et al., 2014; Dugre-Brisson et al., 2005; de Lucas et al., 2014; Jeong et al., 2019; Sugimoto et al., 2015) and decay (Kim et al., 2005; Kim et al., 2007). STAU1, via the post-transcriptional regulation that it imposes to its bound mRNAs, regulates a wide range of physiological transcripts and metabolic pathways. STAU1 is crucial for cell differentiation (Kim et al., 2005; Belanger et al., 2003; Gautrey et al., 2008; Yamaguchi et al., 2008; Gong et al., 2009; Kretz, 2013; Cho et al., 2012), dendritic spine morphogenesis (Vessey et al., 2008; Lebeau et al., 2008), long-term synaptic plasticity (Lebeau et al., 2008), a cellular mechanism for long-term memory, response to stress (Thomas et al., 2009) and cell proliferation (Boulay et al., 2014). In addition, misregulation of STAU1-mediated post-transcriptional mechanisms of gene regulation accelerates cancer progression and regulates apoptosis (Xu et al., 2015; Xu et al., 2017; Liu et al., 2017; Damas et al., 2016; Sakurai et al., 2017).

Interestingly, STAU1 expression levels vary during the cell cycle (Boulay et al., 2014). STAU1 levels rapidly decrease as cells transit through mitosis. Its degradation is mediated by the ubiquitin-proteasome system following its association with the E3 ubiquitin ligase anaphase-promoting complex/cyclosome (APC/C) via its co-activators CDH1 and CDC20 (Boulay et al., 2014). Therefore, modulation of STAU1 levels by cell cycle effectors could dictate the post-transcriptional expression of its bound transcripts and contribute to the control of cell proliferation. Accordingly, moderate overexpression of STAU1 in cancer cells impairs mitosis progression and cell proliferation (Boulay et al., 2014; Wan et al., 2004). Strikingly, STAU1 overexpression has no effect in non-transformed hTERT-RPE1 or IMR90 cells (Boulay et al., 2014), indicating that the types and importance of cellular defects following modulation of STAU1 levels depend on cellular context. Nevertheless, STAU1 is also likely to play an important role during mitosis in non-transformed cells because its depletion impairs mitosis progression (Ghram et al., 2020).

To understand the role of STAU1 during mitosis, we first documented its subcellular distribution, revealing that an important

[1]Département de biochimie et médecine moléculaire, Faculté de médecine, Université de Montréal, 2900 Édouard Montpetit, Montréal, QC H3T 1J4, Canada. [2]Institut de Recherches Cliniques de Montréal, 110 Avenue des Pins Ouest, Montréal, QC H2W 1R7, Canada.
*The first two authors should be regarded as Joint First Authors

‡Author for correspondence (luc.desgroseillers@umontreal.ca)

L.D., 0000-0002-1511-8998

Handling Editor: Maria Carmo-Fonseca
Received 1 April 2020; Accepted 7 June 2020

Journal of Cell Science (2020) 133, jcs247155. doi:10.1242/jcs.247155

subpopulation of STAU1 associates with the mitotic spindle. Previous studies have shown that mRNAs can be found on mitotic spindles (Eliscovich et al., 2008; Groisman et al., 2000; Sharp et al., 2011; Blower et al., 2007; Sepulveda et al., 2018; Kingsley et al., 2007; Hussain et al., 2009) but the mechanisms of their transport, localization and post-transcriptional regulation are unclear. We now show that STAU1 is involved in RNA localization on the spindle. Using RNA-Seq analysis, we identified RNAs that are enriched on spindles, in particular the 45S precursor ribosomal RNA (pre-rRNA) precursor and multiple mRNAs. Interestingly, the pre-rRNA and several mRNAs are delocalized from spindles in HCT116 STAU1-knockout (STAU1-KO) cells compared with wild-type (WT) cells. To conclude, we show that STAU1 partly co-localizes with O-propargyl-puromycin (OP-puromycin), a marker of active translation, on mitotic spindles. Together, our results suggest that STAU1 regulates the transport and localization of different RNA biotypes and that it might contribute to ribosomal RNA maintenance during mitosis and, thus, to nucleolus reassembly.

RESULTS

Localization of STAU1 to the mitotic spindle

To visualize the subcellular localization of STAU1 during mitosis, colorectal cancer HCT116 cells (Fig. 1) and non-transformed hTERT-RPE1 cells (Fig. S1) were synchronized in late G_2 by the CDK1 inhibitor RO-3306 and then released from the block with fresh medium. At different time points post-release, cells were solubilized with Triton X-100, then fixed and stained with anti-STAU1 and anti-α-tubulin antibodies. DAPI staining was included to visualize DNA. Confocal microscopy analysis of mitotic cells revealed that a significant subpopulation of STAU1 co-localized with α-tubulin on the mitotic spindle (Fig. 1A,B). During all phases of mitosis, STAU1 was observed at the poles of the spindle and also on fibers. During telophase, STAU1 was distributed in the cytoplasm of daughter cells and partly with the remains of polar spindle microtubules. Several controls were included to confirm the specificity of the antibodies (Fig. S2).

Biochemical characterization of the mitotic spindle

To confirm a tight association between STAU1 and components of the mitotic spindle, we biochemically purified spindles (Fig. S3A) and identified associated proteins by western blotting (Fig. 2B; Fig. S3B). To prepare spindles, HCT116 and hTERT-RPE1 cells were synchronized in late G_2 and released. Mitotic cells were incubated with taxol (Fig. 2A) to stabilize microtubules and then harvested by shake-off. Purified spindles were observed by microscopy to control for the quality of the preparations (Fig. S3C). Western blot analysis showed that $STAU1^{55}$ was co-purified with tubulin in spindle preparations of both cancer (Fig. 2B) and non-transformed (Fig. S3B) cells. Interestingly, the $STAU1^{63}$ isoform was not detected in the mitotic spindle fraction nor the paralogue protein Staufen2 (STAU2). As expected, aurora A, a known component of the spindle, was found in the spindle fraction whereas calnexin, β-actin and histone H3 used as negative controls were absent. As a further characterization of the spindle preparations, we showed that the ribosomal proteins S6 (RPS6) and L26 (RPL26) co-purified with spindles, suggesting that both the large and small subunits of the ribosomes, and thus the translation machinery, were present in spindle preparations.

dsRBD2 is necessary and sufficient to link $STAU1^{55}$ to spindles

As the first step in defining how $STAU1^{55}$ binds to spindle components, we evaluated the spindle-targeting properties of STAU deletion mutants in order to map spindle association determinants. We first generated STAU1-KO HCT116 cell lines (Fig. S4A-F) to prevent putative dimerization between exogenously expressed $STAU1^{55}$ mutants and endogenous STAU1 (Martel et al., 2010). The growth rate of STAU1-KO (clone CR1.3) HCT116 cells was similar to that of WT cells (Fig. S4D). We then showed that transiently expressed $STAU1^{55}$-$FLAG_3$ co-localized with spindles (Fig. S5A) and was co-purified in spindle preparations (Fig. S5B) from STAU1-KO or STAU1-control WT cells. Then, $STAU1^{55}$-$FLAG_3$ deletion mutants (Fig. 3A) were expressed and their presence in the spindle fraction analyzed by western blotting (Fig. 3B,C). Mutants that lost RNA-binding activity (3*4* and Δ3 in Fig. 3B) (Luo et al., 2002) were present in the spindle fraction, indicating that RNA-binding activity is not required for spindle association. These results were consistent with our findings that $STAU1^{55}$ co-purified with spindles even when spindle preparations were treated with RNase prior to western blotting (Fig. S6). Similarly, deletion of the tubulin-binding domain (ΔTBD) had no effect on the interaction with mitotic microtubules. Deletion of RBD4 or RBD5 (Δ4 and Δ5, respectively, in Fig. 3) had no consequence either. In contrast, a deletion that removed the first N-terminal 88 amino acids of $STAU1^{55}$-$FLAG_3$, corresponding to RBD2 (Δ2 in Fig. 3), reduced $STAU1^{55}$ association with mitotic spindles. The reverse experiment in which RBD2-HA_3 and RBD4-TBD-HA_3, used as control, were expressed in HCT116 STAU1-KO cells confirmed these results (Fig. 4A-C): RBD2-HA_3 was found in the spindle fraction but not RBD4-TBD-HA_3. The results indicate that RBD2 is necessary and sufficient for STAU1–spindle association.

To map more finely the molecular determinant involved in $STAU1^{55}$–spindle association, progressive deletions were made in the N-terminal region and the resulting proteins tested for their capacity to co-purify with spindles (Fig. 4D-F). Western blotting of spindle-associated proteins showed that deletion of the first 25 residues (Δ25) of $STAU1^{55}$ did not prevent $STAU1^{55}$ association with the spindle whereas deletion of the first 37 N-terminal residues (Δ37) abrogated this association. These results indicate that the molecular determinant involved in $STAU1^{55}$–spindle association is located within amino acids 26 and 37.

Transcriptomes of WT and STAU1-KO cells

Given the well-established and conserved role of STAU1 in the regulation of post-transcriptional gene expression, it is likely that $STAU1^{55}$ is responsible for the transport and/or localization of specific RNAs to the spindle as well as for their post-transcriptional regulation while associated with this structure. Therefore, to highlight a putative role of $STAU1^{55}$ in the transport of RNAs to spindles, we biochemically purified mitotic spindles from parental WT and STAU1-KO cells and identified spindle-associated RNAs by RNA-Seq (Table S1). Total RNAs from WT and STAU1-KO mitotic cells were also sequenced to normalize for putative changes in cell transcriptomes as a result of STAU1 ablation. RNA Pico chips analysis showed the quality of RNA preparations (Fig. S7) and a principal component analysis (PCA) plot (Khatua et al., 2003) showed that sequencing data were grouped together according to the source of RNA preparations used (spindle preparations or cell extracts), indicating reproducibility of the replicates (Fig. S8A). The results also indicate that data from whole-cell RNA preparations are different from those from mitotic spindle preparations. Similar conclusions were reached from the calculation of coefficients of correlation between samples (Fig. S8B-E).

Comparison of RNA biotypes in total cell extracts (Fig. 5A) indicated that the relative expression of RNA types per million reads

Journal of Cell Science (2020) 133, jcs247155. doi:10.1242/jcs.247155

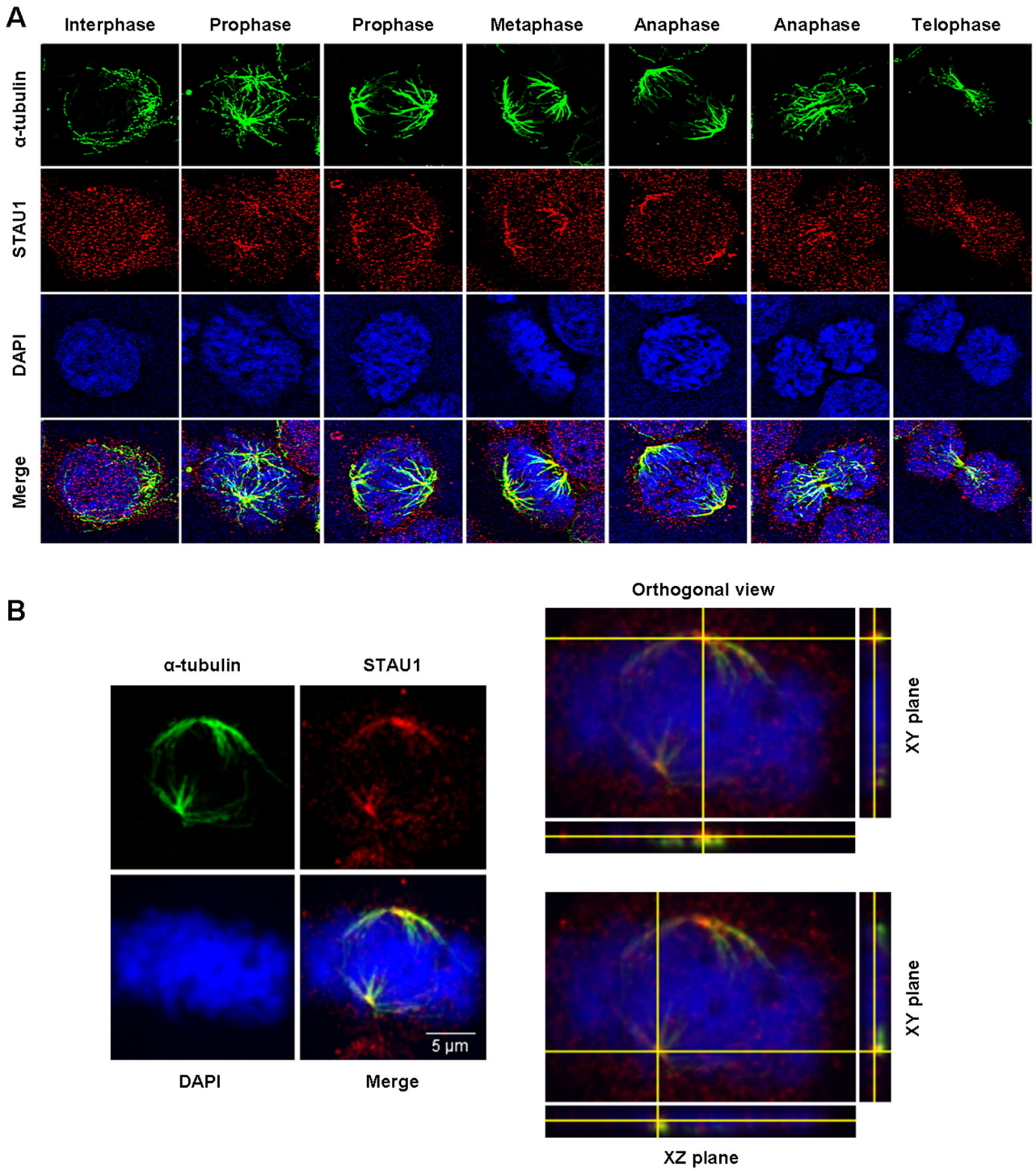

Fig. 1. Localization of STAU1 on the mitotic spindle. HCT116 cells were synchronized in late G2 with the CDK1 inhibitor RO-3306 and released from the block to reach mitosis. Mitotic spindle microtubules were stabilized by Taxol. Cells were solubilized with Triton X-100 before fixation to remove soluble material. (A) Confocal images of cells stained with antibodies against STAU1 and α-tubulin. DNA was stained with DAPI. Cells at different stages of mitosis are shown. This figure is representative of multiple experiments done by three different experimenters. STAU localization on spindles was observed in all mitotic cells. (B) Left: Confocal images of cells stained with antibodies against STAU1 and α-tubulin to visualize STAU1 and mitotic spindles. DNA was stained with DAPI. Right: 3D-analysis of the relative position of STAU1 and α-tubulin on microtubules shows co-localization of the proteins in space.

in the transcriptomes of WT and STAU1-KO cells was similar (Table 1). Almost half of the reads corresponded to protein-coding RNAs. Using a fragments per kilobase of transcript per million (FPKM) of 1 as a threshold value for gene expression, only 108 individual RNAs were found to have altered expression in STAU1-KO cells compared with WT cells (fold change ≥2, adjusted *P*-value ≤0.05; Table S1). A total of 35 protein-coding mRNAs and four long non-coding RNAs (lncRNAs) were upregulated, whereas 68 protein-coding mRNAs and one lncRNA were downregulated (Table S2).

Journal of Cell Science (2020) 133, jcs247155. doi:10.1242/jcs.247155

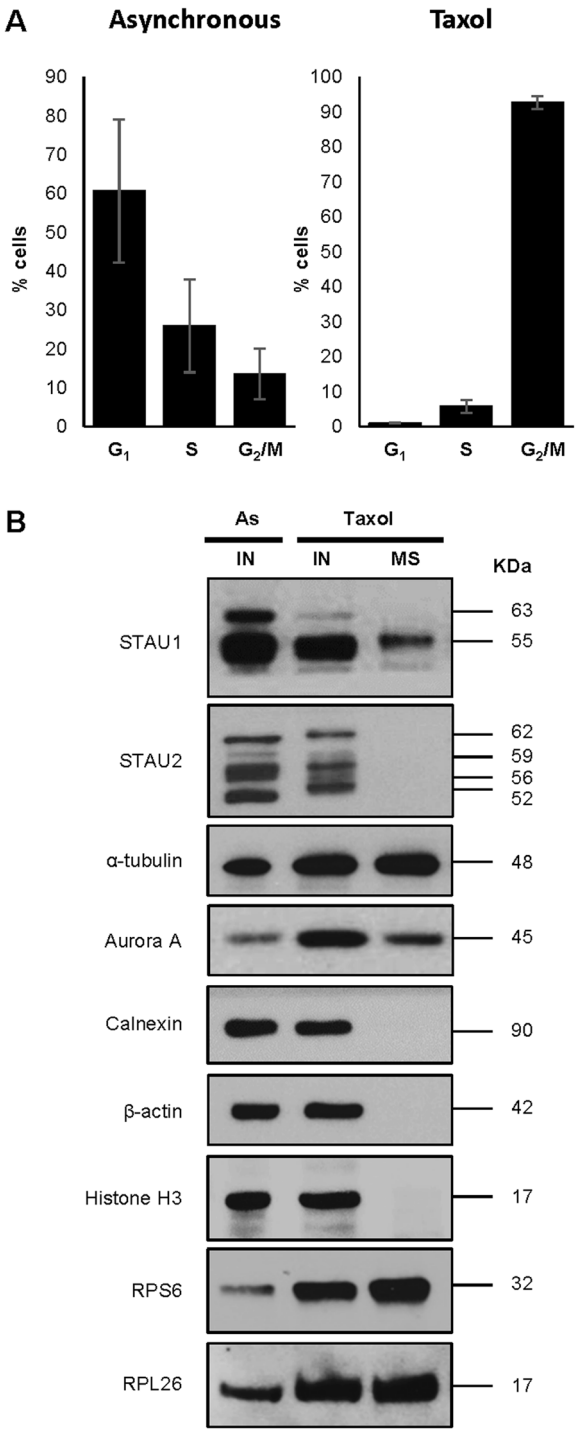

Fig. 2. Co-purification of STAU1 with mitotic spindle proteins. (A) Cell cycle distribution of unsynchronized (Asynchronous) and taxol-synchronized (Taxol) cells was determined by FACS analysis ($P \leq 0.05$; Student's *t*-test; $n=3$). (B) Western blot analysis of purified mitotic spindles (MS) using specific antibodies. Total input lysates (IN) from asynchronous (As) and taxol-synchronized (Taxol) cells were loaded as controls. This figure is representative of three independently performed experiments.

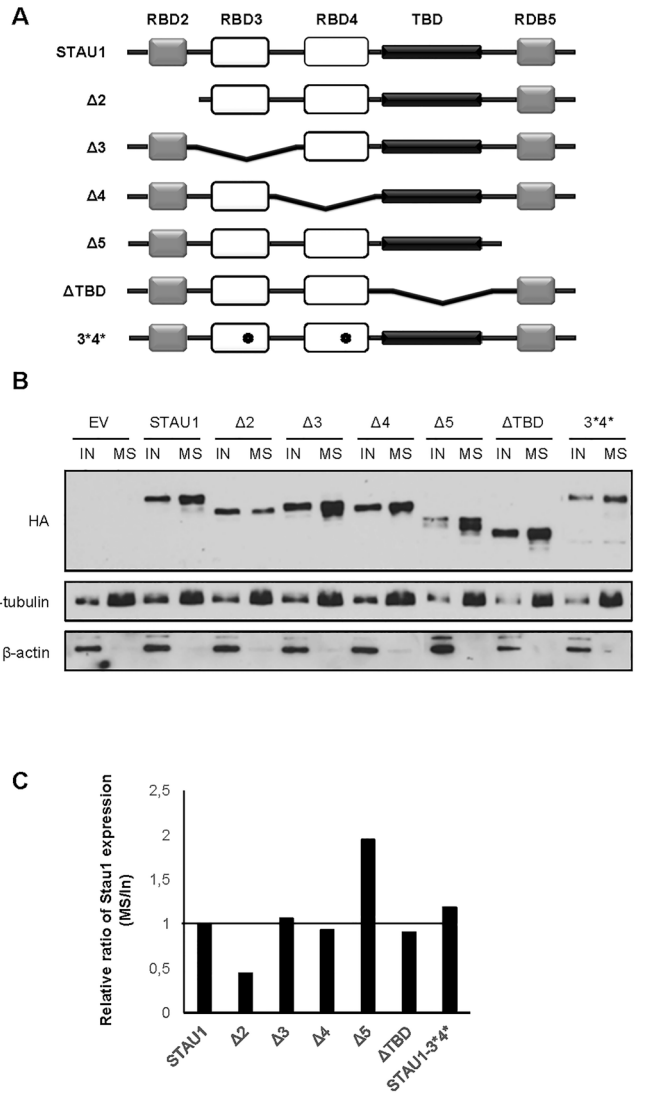

Fig. 3. Mapping of the molecular determinant involved in STAU1–spindle association. STAU1-KO HCT116 cells were transfected with plasmids coding for HA_3-tagged STAU1 WT or deletion mutants (Δ) to map the molecular determinant involved in the binding of STAU1 to the mitotic spindle. (A) Representation of STAU1 WT and mutants. * indicates mutation that abolishes STAU1 RNA-binding activity. RBD: RNA-binding domain. TBD, tubulin-binding domain. White boxes, RNA-binding domains. Gray boxes, domains that do not bind RNA *in vitro* although they have the consensus sequence for RNA binding. Black boxes, tubulin-binding domains. (B) Cells were synchronized in mitosis with taxol. Proteins from the total cell extracts (IN) and from purified spindle preparations (MS) were analyzed by western blotting. Proteins were identified with specific antibodies as indicated. (C) Quantification of STAU1 proteins on the mitotic spindle. The ratio of STAU1 amounts in the spindle preparations over that in the total mitotic cell extracts was calculated. The ratio obtained for STAU1 WT was arbitrarily fixed to 1. These data are representative of two independently performed experiments that gave similar results.

Genome-wide identification of mitotic spindle-enriched RNAs

A different pattern was observed with spindle preparations (Fig. 5A, Table 1). The relative expression per million reads (transcripts per million, TPM) of protein-coding RNAs was higher in mitotic spindle preparations from STAU1-KO cells than from WT cells, whereas those of micro-RNAs (miRNAs) and ribosomal RNAs (rRNAs) were lower. Strikingly, the huge decrease in miRNAs and rRNAs was essentially due to three highly abundant RNAs in spindle preparations, RNA28S5, mir3648 and mir3687 (Table 1). Interestingly, the chromosomal location of mir3648 and mir3687 was within the RNA28S5 45S pre-rRNA locus (Fig. 5B), suggesting that the two miRNA sequences are present in spindle

Journal of Cell Science (2020) 133, jcs247155. doi:10.1242/jcs.247155

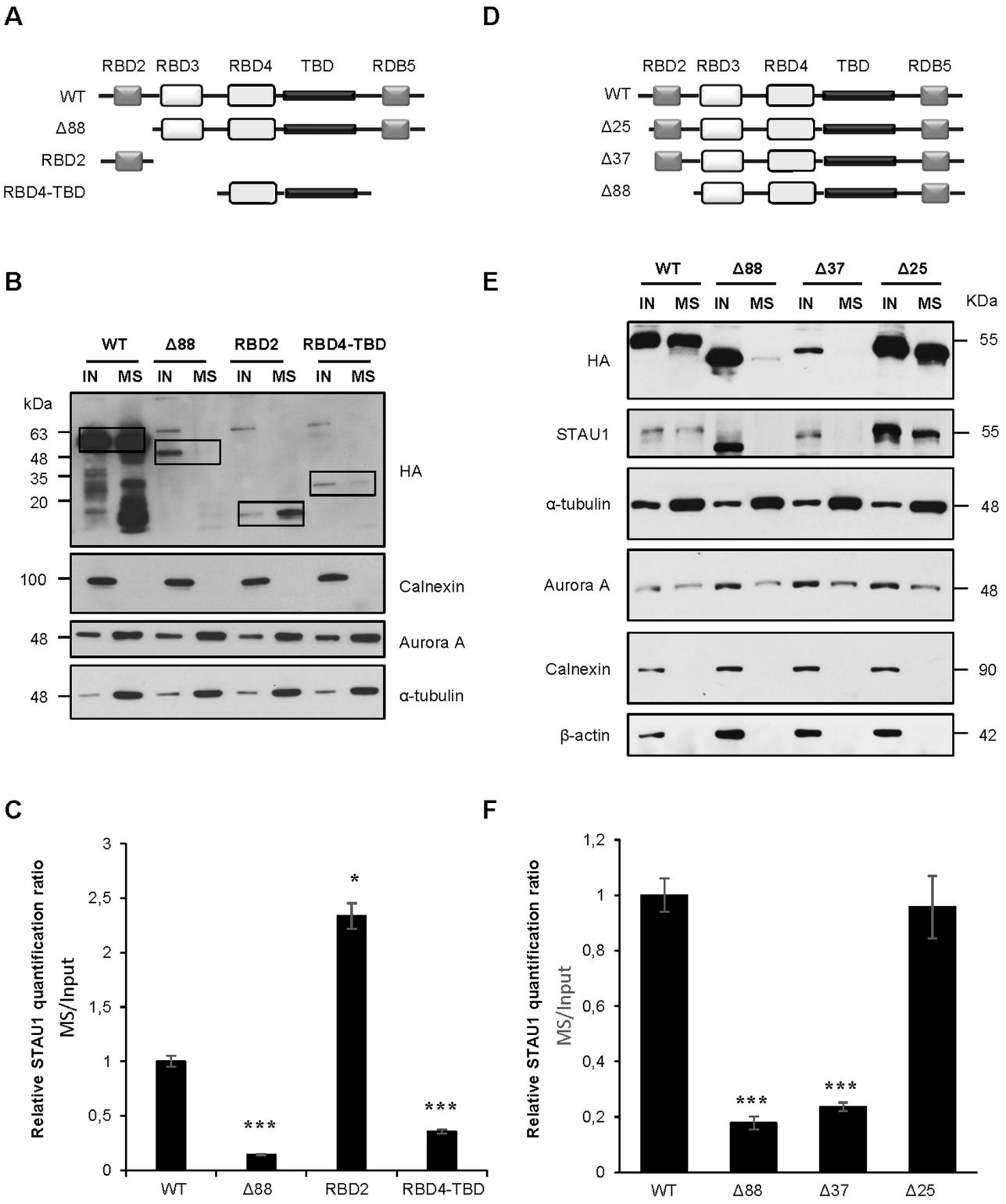

Fig. 4. Fine mapping of the *N*-terminal determinant responsible for STAU1–spindle association. (A,D) Representations of STAU1 deletion mutants (see legend of Fig. 3A for box codes). (B,E) Proteins from total cell extracts (IN) and purified spindle preparations (MS) were analyzed by western blotting with specific antibodies. (C,F) Quantification of the amounts of STAU1 proteins on the mitotic spindle. The ratio of STAU1 amounts in the spindle preparations over that in the cell extracts was calculated. Graphs show the mean±s.d. of three independently performed experiments. The ratio obtained for STAU1 WT was arbitrarily fixed to 1. *$P \leq 0.05$, ***$P \leq 0.001$ (one sample *t*-test).

preparations within the pre-rRNA transcript and not as mature miRNAs. This huge decrease in the number of reads (TPM) of rRNAs and miRNAs in STAU1-KO spindles compared with WT spindles resulted in over-representation of all other RNA biotypes, including protein-coding transcripts (Table 1). To confirm the presence of pre-rRNA in spindle preparations, we used real-time

Journal of Cell Science (2020) 133, jcs247155. doi:10.1242/jcs.247155

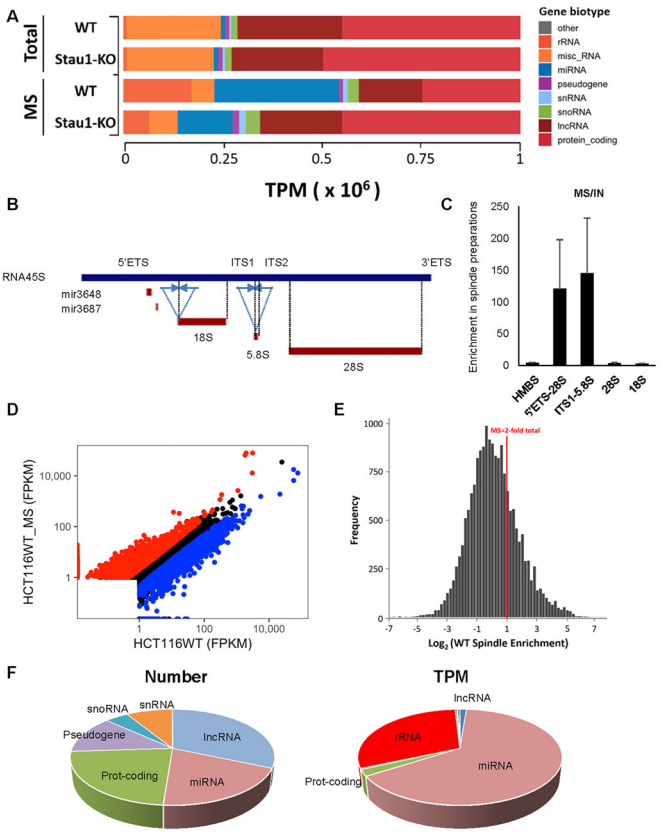

Fig. 5. Spindle-enriched transcriptome in HCT116 cells. (A) Histogram depicting the RNA biotype content, in transcripts per million (TPM), in total mitotic cell extracts (Total) and mitotic spindles (MS) from WT and STAU1-KO HCT116 cells. Biotypes accounting for less than 1% of the overall TPMs were grouped as 'other'. (B) Representation of the RNA28S5 locus showing the 45S pre-rRNA. Arrows indicate the position of the oligonucleotides used for RT-qPCR, as shown in C. The position of miRNAs and mature rRNAs is shown. (C) RT-qPCR amplification of spindle-associated RNAs using oligonucleotides that recognized different parts of the 45S rRNA. The levels of enrichment in spindle preparations (MS) compared with cell extracts (IN) are shown. The graphs show the mean±s.d. of three independently performed experiments. HMBS, hydroxymethylbilane synthase; ETS, external transcribed spacer; ITS, internal transcribed spacer. (D) Scatter plots of the relative distribution of FPKM mapped reads in mitotic spindle preparations (MS) versus cell extracts from WT HCT116 cells. Red, RNAs at least twofold more abundant (P≤0.05) in MS than in cell extracts. Blue, RNAs at least twofold less abundant (P≤0.05) in MS than in cell extracts. (E) Histogram of the frequency of genes as a function of their enrichment in MS preparations versus cell extracts from WT cells. (F) Relative amount of RNAs delocalized from the spindle in the absence of STAU1-KO cells. The percentages of the number of different individual RNA in each biotype (left) and the percentage of TPM in each biotype (right) are shown.

quantitative PCR (RT-qPCR) to amplify spindle-associated RNAs with oligonucleotide primers positioned on either side of the 5′ETS/18S and ITS1/5.8S junctions (Fig. 5B). Our results indicated that the spacer fragments were linked to ribosomal sequences and therefore that the pre-rRNA was highly enriched in spindle preparations (Fig. 5C). Sequences corresponding to mature 18S and 28S rRNAs were also very abundant in the spindle preparations, but they were not enriched compared with input because they were also present as abundant cytoplasmic ribosomes. These results indicate that the precursor 45S rRNA is an important component of the spindle transcriptome.

Table 1. Total number of individual transcripts and of transcripts per million across RNA biotypes

		TPM			
Biotype	Number	MS-CR1.3	MS-WT	IN-CR1.3	IN-WT
lncRNA	2549	177,538	132,034	224,053	256,876
miRNA	711	137,876	313,748	10,511	10,185
misc_RNA	395	71,640	58,060	219,190	237,103
Protein coding	11,782	449,509	247,028	497,031	449,242
Pseudogene	1545	16,440	10,274	11,315	10,531
rRNA	19	64,205	170,341	8024	8372
snoRNA	361	64,869	55,563	23,091	21,775
snRNA	414	16,651	11,771	5718	5314
tRNA	22	1269	1178	1063	596
RNA28S5	1	62,906	168,792	6030	6090
mir3648	1	45,624	138,997	3033	3562
mir3687	1	85,280	168,002	3869	3828

CR1.3, STAU1-KO HCT116 cells (clone CR1.3); IN, input (total mitotic cell extract); lcnRNA, long non-coding RNA; miRNA, microRNA; MS, mitotic spindle; Number, number of individual RNAs; rRNA, ribosomal RNA; snRNA, small nuclear RNA; snoRNA small nucleolar RNA; TPM, transcripts per million; tRNA, transfer RNA; WT, wild type HCT116 cells.

We then identified other spindle-enriched RNAs in WT cells. We plotted the amount of each RNA (FPKM) in the mitotic spindle preparations as a function of their amount in total cell extracts (Fig. 5D) and analyzed the frequency of RNAs as a function of their enrichment in mitotic spindle preparations compared with cell extracts (Fig. 5E). These results identified 1642 RNAs that were enriched at least twofold (P≤0.05) in spindle preparations compared with total cell extracts, including 1054 protein-coding transcripts (Table S3, S4). Of these mRNAs, 28% are known to bind STAU1 (Furic et al., 2008; Boulay et al., 2014; Ricci et al., 2014; Sugimoto et al., 2015; de Lucas et al., 2014). These mRNAs code for proteins involved in cellular processes such as cell differentiation, GTPase activity, microtubule-based processes and chromatin organization and modification (Table S5). In addition, the pre-rRNA as well as small nucleolar RNAs (snoRNAs) involved in pre-rRNA processing and MALAT1, a scaffold lncRNA involved in ribonucleoprotein assembly, were highly enriched (Table S3).

STAU1^{55}-mediated localization of RNAs on mitotic spindle

To identify RNAs whose localization to the spindle is dependent on STAU1, we compared the amount of individual RNA in spindle preparations of WT and STAU1-KO cells. We normalized the amount of each RNA in the spindle preparations to that in cell extracts (RNA-spindle/RNA-input) and then compared the ratios in STAU1-KO versus WT cells. We identified 771 individual RNAs, including RNA28S5, miRNAs (including mir3648 and mir3687) and 154 protein-coding mRNAs whose amount in the spindle preparations was at least two-fold lower for STAU1-KO cells than for WT cells (Fig. 5F; Table S6). A different pattern appeared with the analysis of TPM: the most important decrease concerns the pre-rRNA and its associated miRNAs whereas protein-coding transcripts represented only 2% of the total decreased reads (Fig. 5F). Of the protein-coding mRNAs, 29.2% are known to bind STAU1. Among the remaining mRNAs that do not bind STAU1, 60% (60/109) were only marginally expressed (FPKM<2). Bioinformatic analysis using 'Metascape, A Gene Annotation & Analysis Resource' (Tripathi et al., 2015) indicated that the proteins encoded by these STAU1-bound mRNAs were enriched in GO terms related to regulation of cell shape, actin-cytoskeleton

Journal of Cell Science (2020) 133, jcs247155. doi:10.1242/jcs.247155

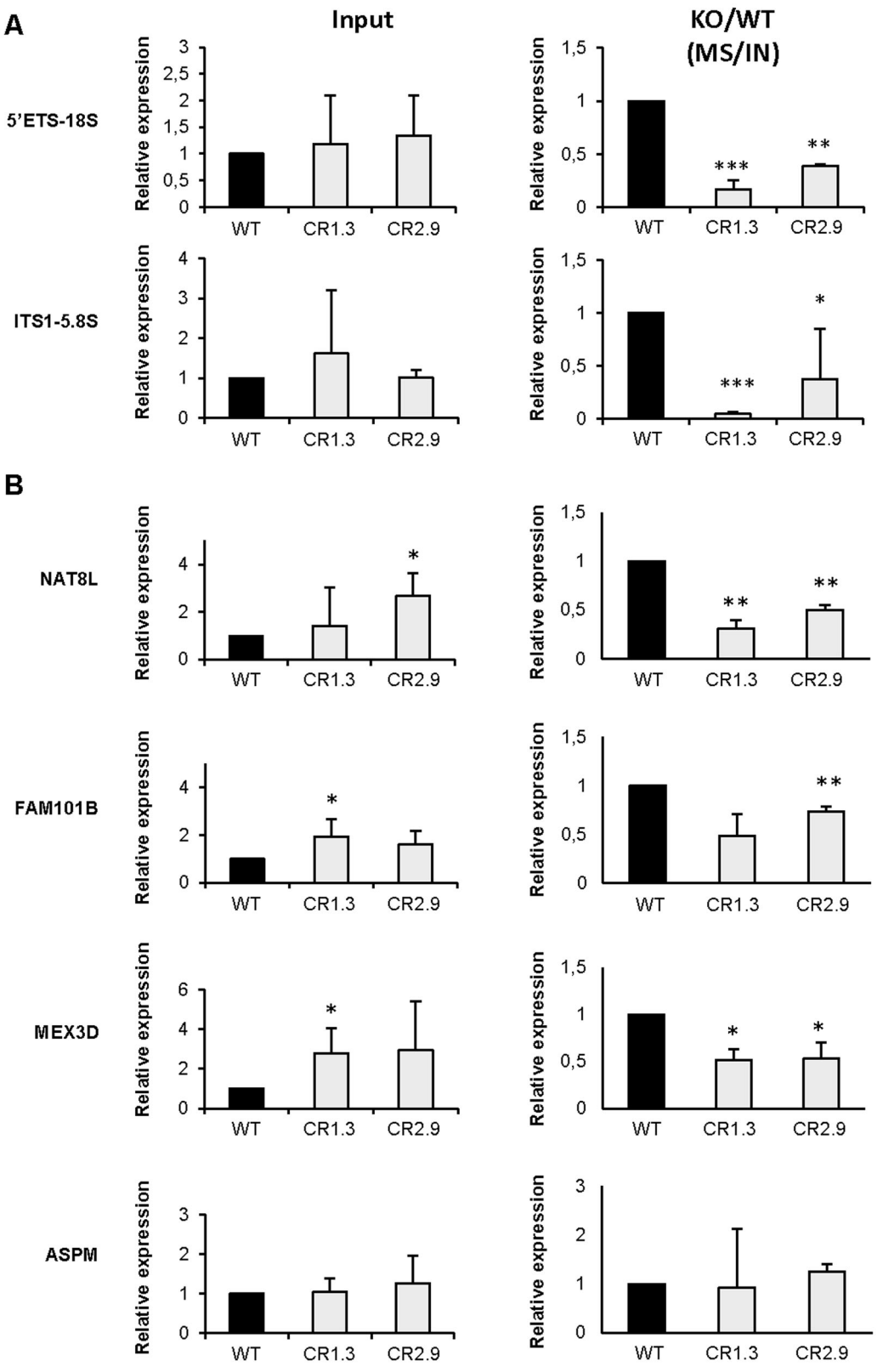

Fig. 6. See next page for legend.

organization, negative regulation of cell growth and differentiation (Table S7).

To confirm the STAU1-mediated differential association of RNAs with spindles of WT and KO cells, selected RNAs were quantified in cell extracts and spindle preparations from WT and STAU1-KO cells by RT-qPCR. Two different STAU1-KO cell lines, generated with different guide RNAs (Fig. S4), were used to exclude putative off-target effects. Based on RNA-Seq data, we

Journal of Cell Science (2020) 133, jcs247155. doi:10.1242/jcs.247155

Fig. 6. Validation of RNA-Seq data by RT-qPCR. WT and STAU1-KO HCT116 cells were synchronized in mitosis. Two STAU1-CRISPR-KO cell lines (CR1.3 and CR2.9) generated with different RNA guides were used. RNAs in mitotic cell extracts (left) and in purified mitotic spindle preparations (right) were analyzed. RNAs were quantified by RT-qPCR with specific primer pairs. (A) The contribution of STAU1 in pre-rRNA localization. Graphs show the mean±s.d. of three independently performed experiments. *$P\leq0.05$, **$P\leq0.01$, ***$P\leq0.001$ (one sample *t*-test). (B) The amount of mRNAs in cell extracts and in spindle preparations expressed as the ratio of the amount of a specific gene over that of the negative controls HPRT+RPL22. The ratios obtained with RNAs in the spindle preparations were normalized to the ratio in the cell extracts in both STAU1-KO and WT cells. The ratio for WT cells was arbitrarily fixed to 1. Graphs show the mean±s.d. of four independently performed experiments. ASPM, abnormal spindle microtubule assembly; MEX3D, mex-3 RNA-binding family member D; FAM101B, refilin B; NAT8L, *N*-acetyltransferase 8 like; HPRT, hypoxanthine guanine phosphoribosyl transferase; RPL22, ribosomal protein L22.

studied several RNAs whose amounts were decreased in spindle preparations of STAU1-KO cells compared with WT cells and are known targets of STAU1 binding. *Hprt* and *rpl22* mRNAs were used as negative controls to normalize data. As expected from RNA-Seq data, the 45S precursor rRNA was delocalized from the spindles of STAU1-KO cells compared with WT cells (Fig. 6A), as were *mex3d*, *fam101b* and *nat8 l* mRNAs (Fig. 6B). Used as control, the level of *aspm* RNA was unchanged in STAU1-KO spindle extracts compared with WT extracts.

STAU1^{55} co-localizes with ribosomes and OP-puromycin on the mitotic spindle

The biochemical characterization of spindle-associated proteins indicated that ribosomal proteins were co-purified with tubulin and STAU1^{55} in spindle preparations (Fig. 2). To study the link between ribosomes, spindles and STAU1^{55}, we documented their subcellular localization during mitosis (Fig. 7). Using confocal microscopy, we first showed that a significant subpopulation of the ribosomal protein S6 co-localized with tubulin (Fig. 7A) and with STAU1 (Fig. 7B) on the mitotic spindle both at the poles and on fibers. Then, we treated cells with OP-puromycin, a marker of active translation (Chao et al., 2012). The signal was detected by confocal microscopy along with those generated by anti-tubulin and anti-STAU1 antibodies (Fig. 7C). Our results indicate that foci of OP-puromycin co-localize with subpopulations of both tubulin and STAU1 on the mitotic spindle of individual cells.

DISCUSSION

In this paper, we show that STAU1^{55} associates with the mitotic spindle in both transformed HCT116 and non-transformed hTERT-RPE1 cells. STAU1^{55} is present in mitotic spindle preparations and co-localizes with tubulin and ribosomes on the mitotic spindle. This is consistent with previous large-scale proteomic studies that identified STAU1 as a spindle component of the human (Rao et al., 2016) and hamster (Bonner et al., 2011) mitotic apparatus. In contrast, STAU1^{63} was not found in spindle preparations. This was unexpected because the sequence of STAU1^{55} is entirely included in that of STAU^{63} (Wickham et al., 1999). It is likely that the additional amino acids at the N terminus of STAU^{55} to generate STAU1^{63} change the structure of the molecular determinant involved in STAU1^{55} association with the spindle and make it inaccessible for protein interaction. Similarly, the paralogue STAU2 is not associated with the spindle, consistent with recent observations that failed to localize STAU2 to the mitotic spindle, although it co-localizes with the spindle at meiosis I and II (Cao et al., 2016). The human paralogues independently evolved from an ancestor gene and acquired differential biological functions while keeping conserved molecular characteristics. Although the human paralogues are both RNA-binding proteins, they bind mainly different sets of mRNAs (Furic et al., 2008) and are essentially present in distinct ribonucleoprotein complexes (Duchaine et al., 2002). Accordingly, they play different roles in spines morphogenesis (Lebeau et al., 2008; Goetze et al., 2006) and synaptic activity (Lebeau et al., 2008; Lebeau et al., 2011). Interestingly, in *Drosophila* embryos, Staufen protein moves to the pole of the mitotic spindles in close association with the astral microtubules when bicoid 3′UTR mRNA is injected (Ferrandon et al., 1994).

Molecular determinant involved in STAU1^{55}–spindle association

STAU1 is a multifunctional protein with several determinants that control its molecular functions. Notably, RBD3 and RBD4 regulate STAU1 RNA-binding activity (Wickham et al., 1999) and RBD4-TBD is involved in ribosome association (Luo et al., 2002). We now show that STAU1 association with spindles requires the N-terminal region that contains RBD2, a domain devoid of RNA-binding activity *in vitro* (Wickham et al., 1999), although we do not exclude the possibility that RBD2 could bind RNA *in vivo* as reported for the paralogue protein STAU2 (Heber et al., 2019). This result indicates that STAU1 RNA-binding and ribosome-binding activities are not involved in spindle association. It is interesting to note that deletion of the C-terminal RBD5 facilitates RBD2–spindle association (Figs 3, 4). This is consistent with previous data showing an interaction between RBD2 and RBD5 (Martel et al., 2010) and indicates that RBD5 might regulate the functions of RBD2. RBD2 was also shown to bind CDC20 and CDH1, resulting in STAU1 ubiquitylation and degradation during mitosis (Boulay et al., 2014), and to be required for impaired cell proliferation (Boulay et al., 2014). In addition, the region of RBD2 involved in STAU1–spindle association (amino acids 25-37) is also required to increase Pr55^{Gag} multimerization and HIV particle release (Chatel-Chaix et al., 2008), suggesting that HIV Gag highjacks STAU1 function to favor its own replication. Understanding the role of STAU1 on the mitotic spindle is crucial, not only to decipher new pathways leading to cell proliferation but also to discover new steps in RNA virus replication and therefore novel approaches to interfere with them.

The mechanism by which the N-terminal determinant (M^{26}RGGAYPPRYFY^{37}) allows STAU1^{55} association with spindles is not known. Interestingly, in *Drosophila*, a proline-rich loop in *Drosophila* RBD2 is required for the microtubule-dependent localization of *osk* mRNA but not for Staufen association with *osk* mRNA or for activation of its translation (Micklem et al., 2000). It will be of interest to test whether P32-P33 are involved in this process and/or whether mutations that prevent tyrosine phosphorylation (Y35 and Y37) or arginine methylation (R27 and R34) (Hornbeck et al., 2015) impair STAU1^{55}–spindle association. Alternatively, the N-terminal motif might recruit ubiquitin ligase through two potential ESCRT targeting domains (P^{32}PRY and Y^{37}PFVPPL) that, in turn, target the protein to the ESCRT machinery. Interestingly, several ESCRT proteins localize to mitotic microtubules and play important roles throughout mitosis in centrosome localization and duplication, spindle organization and stability, kinetochore attachments, spindle checkpoint, nuclear envelope reassembly and cytokinesis (Dionisio-Vicuna et al., 2018; Morita et al., 2010; Petsalaki et al., 2018; Petsalaki and Zachos, 2018; Vietri et al., 2015).

Journal of Cell Science (2020) 133, jcs247155. doi:10.1242/jcs.247155

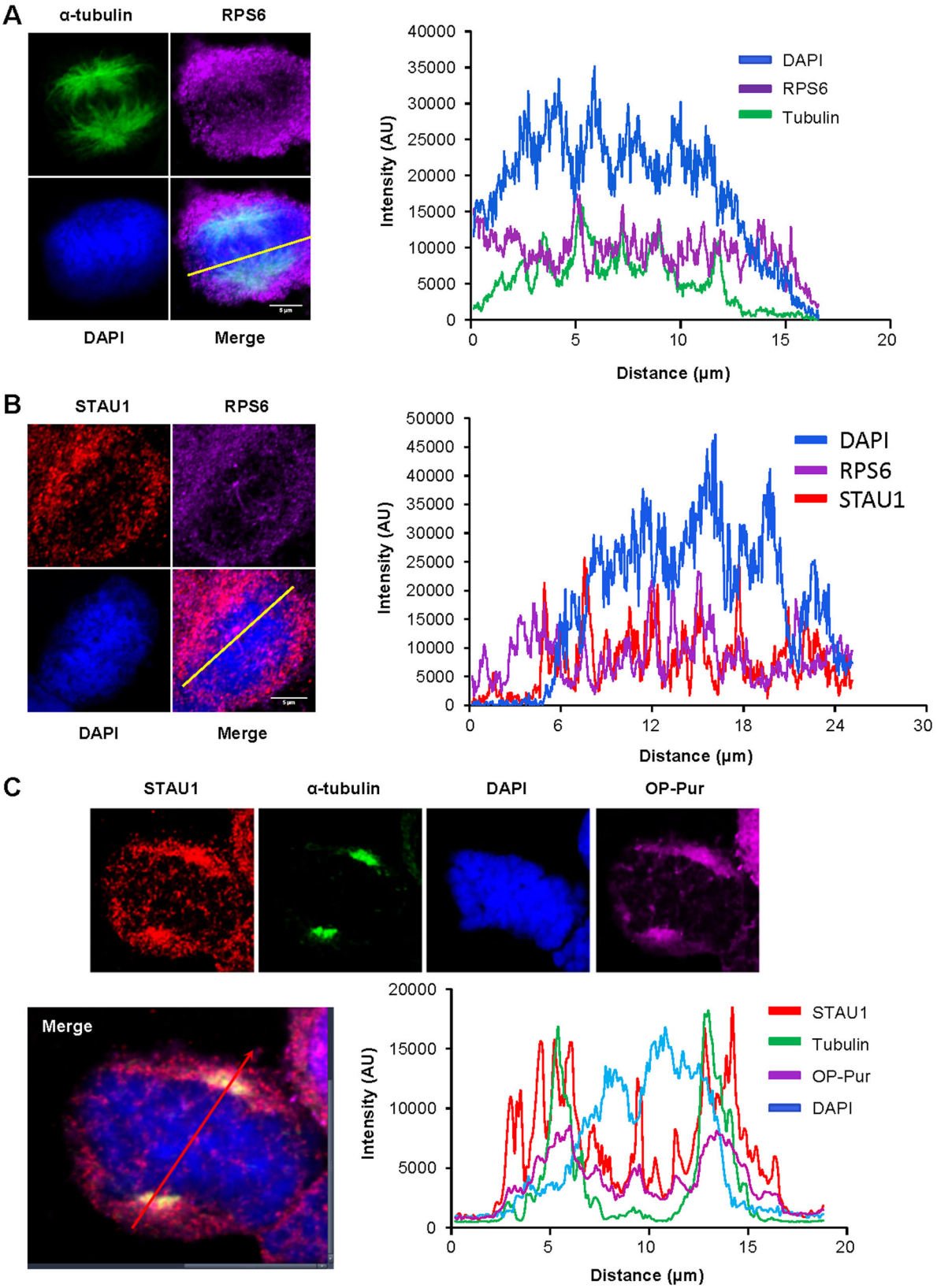

Fig. 7. See next page for legend.

Spindle-enriched RNAs

Large-scale RNA-Seq experiments identified RNAs that were enriched in spindle preparations compared with total cell extracts, including many protein-coding transcripts (Table S3) (Blower et al., 2007). The fate of these transcripts is not clear. Although it is accepted that essential proteins required for mitosis are synthesized

Journal of Cell Science (2020) 133, jcs247155. doi:10.1242/jcs.247155

Fig. 7. Co-localization of STAU1 and the translation machinery on spindles. HCT116 cells were synchronized in late G_2 with the Cdk1 inhibitor RO-3306 and released from the block with fresh medium to reach mitosis. Cells were treated with Triton-X 100 to remove soluble materials before fixation. (A) Cells were stained with anti-S6 (RPS6) and anti-tubulin antibodies to localize ribosomes and the mitotic spindle, respectively. DNA was stained with DAPI. Line scan (right) analysis indicates co-localization of RPS6 and tubulin on fiber tracks. The figure is representative of three independently performed experiments giving similar results in every cell. (B) Cells were stained with anti-S6 (RPS6) and anti-STAU1 antibodies to localize ribosomes and STAU1, respectively. DNA was stained with DAPI. Line scan (right) analysis shows overlapping peaks of RPS6 and STAU1 signals. The figure is representative of three independently performed experiments giving similar results in every cell. (C) Cells were stained with anti-tubulin and anti-STAU1 antibodies as well as with O-propargyl-puromycin (OP-Pur), a marker of active translation. DNA was stained with DAPI. Co-localization was quantified by line scan analysis. The figure is representative of five independently performed experiments giving similar results in every cell. Scale bars: 5 µm.

prior to prophase, several studies have shown that mitotic translation (Groisman et al., 2000) and inhibition of cap-dependent translation (Wilker et al., 2007) are important for proper mitotic progression. For example, active translation is needed from late prophase to prometaphase to synthesize proteins that determine the duration of mitosis exit (Cummins et al., 1966). Large-scale ribosome profiling experiments confirmed that proteins are synthesized during mitosis (Stumpf et al., 2013; Tanenbaum et al., 2015; Park et al., 2016; Aviner et al., 2013). However, whether translation occurs on the spindle, in the cytoplasm or both is unknown.

The presence of ribosomes and active sites of translation suggests that translation can occur on the spindle, consistent with the presence of several spindle-associated mRNAs in the lists of proteins that are translated during mitosis (Aviner et al., 2013). Mitotic translation indeed contributes to the protein content of the mitotic apparatus (Blower et al., 2007). Consistently, depletion of several of these spindle-enriched mRNAs by RNA interference impairs normal spindle pole organization and γ-tubulin distribution (Sharp et al., 2011), indicating that local translation of these mRNAs on the spindle is beneficial for mitosis progression. Interestingly, no correlation was established between the spindle-enrichment of specific mRNAs and their translation on the spindle (Sharp et al., 2011). Therefore, it was proposed that some transcripts are spatially translated on spindles whereas others are translationally inactive cargos that are later segregated into daughter cells (Blower et al., 2007).

Strikingly, one of the most abundant RNAs on spindles is RNA28S5, corresponding to the 45S pre-rRNA. This pre-rRNA is transcribed by RNA polymerase I from multiple 45S rDNA repeat units organized into five clusters on different chromosomes. During interphase, pre-rRNA is found in the nucleolus, where it is processed to form mature 18S, 5.8S and 28S rRNAs and assembled into ribosomes (Hernandez-Verdun, 2011). During prophase, the nucleolus disassembles and rDNA transcription as well as pre-rRNA processing is arrested for the time of mitosis. The 45S pre-rRNA is maintained during mitosis and is present in the cytoplasm (Shishova et al., 2011) and at the chromosome periphery together with pre-rRNA processing factors (Sirri et al., 2016; Shishova et al., 2011). During telophase/early G_1, the nucleolus is reassembled and the mitosis-inherited 45S pre-rRNA is required for regulating the distribution of components to reassembling daughter cell nucleoli (Carron et al., 2012; Dundr et al., 2000). Our study now indicates that the pre-rRNA, as well as numerous snoRNAs involved in rRNA maturation, is associated with the mitotic spindle during mitosis, allowing their segregation into the two daughter cells and reassembly of the nucleoli. The presence of full-length pre-rRNA on the spindle contrasts with previous observation in the clam Spisula that only the processed rRNA spacers, but not the full-length precursor, are associated with centrosomes during meiosis (Alliegro and Alliegro, 2013).

STAU1^{55}-dependent localization of mRNAs on the mitotic spindle

Using WT and STAU1-KO cells, we identified RNAs that are delocalized from the spindle when STAU1 is depleted. Because their overall expression in total cell extracts was not changed in STAU1-KO compared with WT cells, these results indicate that STAU1^{55} is responsible for the transport and localization of RNA populations to the spindle. Strikingly, the 45S pre-rRNA accounts for most of the reduced reads that are observed in STAU1-depleted cells, revealing a novel role for STAU1^{55} in nucleolus function and reassembly. STAU1 was previously shown to be associated with ribosomes (Luo et al., 2002) and to enhance translation when bound to the 5′UTR of mRNAs (Dugre-Brisson et al., 2005). In addition, STAU1 was shown to transit through the nucleolus where it is thought to be involved in ribosome and/or ribonucleoprotein biogenesis (Martel et al., 2006). Our results now add an additional putative role of STAU1 in pre-rRNA trafficking during mitosis and nucleolus reassembly in daughter cells.

Trafficking of other RNA populations is also altered in STAU1-KO cells. The number of different protein-coding transcripts represents a relatively small percentage of delocalized RNA molecules (20%) and only 2% of the delocalized reads. We believe that this is an under-representation of the number of delocalized STAU1-bound transcripts because of incorporation of additional reads required to compensate the huge decrease in rRNA reads (TPM) in STAU1-KO spindles compared with WT spindles. The fate of these mRNAs on spindles is unknown. It is likely that a subpopulation of mRNAs on the spindle is locally transcribed. Another subpopulation of STAU1-bound mRNAs is probably sequestered to the spindle in a translationally inactive form, and subsequently released and translated during G_1. Consistently, large-scale ribosomal profiling (Stumpf et al., 2013; Tanenbaum et al., 2015; Park et al., 2016) of G_2, M and G_1 synchronized cells identified over 300 mRNAs whose translation is up- or downregulated during mitosis versus G_1 or G_2, whereas the amounts of their corresponding mRNAs remain unchanged. At least 18 of the 154 mRNAs shown to be delocalized from the mitotic spindle in STAU1-KO cells were among those whose translation is regulated. Interestingly, all of them but one show reduced translation during mitosis. Strikingly, 14 of these 18 mRNAs are known targets of STAU1, suggesting that STAU1 is a crucial factor in a mechanism of translation inhibition during mitosis.

Thus, STAU1 controls, in different cellular compartments, differential subpopulations of pre-rRNAs and mRNAs that probably regulate cell decision during mitosis. The consequence of STAU1 depletion varies according to cellular context. Although it has no observable effect in cancer cells, STAU1 depletion impairs mitosis progression and cell proliferation in non-transformed cells (Ghram et al., 2020). Nevertheless, spindle defects are not observed and both daughter cells survive. It is possible that STAU1 depletion interferes somehow with a mitotic checkpoint control, a mechanism that is often lost in cancer cells. Cancer cells are rather susceptible to STAU1 overexpression (Boulay et al., 2014). Overexpression, which also alters the fate of STAU1-bound mRNAs, hinders cell proliferation via a reduction in the number of cells that transit mitosis. STAU1 regulates crucial functions via the post-transcriptional regulation that it imposes to its bound RNAs, and deregulation of this

Journal of Cell Science (2020) 133, jcs247155. doi:10.1242/jcs.247155

mechanism might explain the proliferation defects observed in non-transformed cells upon STAU1 depletion (Ghram et al., 2020) and in cancer cells upon STAU1 overexpression (Boulay et al., 2014).

MATERIALS AND METHODS

Plasmids and reagents

Plasmids coding for STAU1$^{\Delta 2}$-HA$_3$, STAU1$^{\Delta 3}$-HA$_3$, STAU1$^{\Delta 4}$-HA$_3$, STAU1$^{\Delta 5}$-HA$_3$, STAU1$^{\Delta TBD}$-HA$_3$, STAU1^{3*-4*}-HA$_3$, STAU1$^{\Delta 25}$-HA$_3$ and STAU1$^{\Delta 37}$-HA$_3$, as well as RBD2-HA$_3$ and RBD4-TBD-HA$_3$, were described previously (Luo et al., 2002; Martel et al., 2010; Chatel-Chaix et al., 2008; Wickham et al., 1999; Boulay et al., 2014). Monoclonal (1:1000) and rabbit (1:1000) anti-STAU1 antibodies were described previously (Dugre-Brisson et al., 2005; Rao et al., 2019). Anti-β-actin (A5441, clone AC-74; 1:5000), anti-STAU2 (HPA019155; 1:500), anti-α-tubulin (T6074, batch number 023M4813; 1:40,000) and anti-HA (H6908, batch number 115M4872v; 1:1000) antibodies were purchased from Sigma-Aldrich. Anti-aurora A (30925, batch number 2; 1:2000), anti-α-tubulin (ab18251, batch number GR201260-1; 1:40,000 for IF) and anti-histone H3 (ab1791, batch number GR204148-1; 1:3000) antibodies were purchased from Abcam. Anti-calnexin (sc-11397, batch number C1214; 1:1000) antibody was obtained from Santa Cruz Biotechnology. Anti-RPS6 (2212, batch number 4; 1:1000) was purchased from Cell Signaling Technology. Anti-RPL26, (GTX101833; 1:1000) and anti-STAU1 (GTX106566; 1:200 for IF) was obtained from Genetex. Goat polyclonal anti-mouse (p0447, batch number 20051789; 1:3000) and anti-rabbit (p0448, batch number 20017525; 1:5000) antibodies were purchased from Dako.

Cell culture

The human cell lines hTERT-RPE1 and HCT116 were obtained from ATCC (Manassas, USA). Human colorectal HCT116 cells and STAU1-KO CRISPR-derived clones were cultured in McCoy's medium containing 10% fetal bovine serum, 20 mM glutamine and 1% penicillin–streptomycin (Wisent). The human cell line hTERT-RPE1 was cultured in Dulbecco modified Eagle's medium (Invitrogen) supplemented with 10% Cosmic Calf Serum (HyClone) or fetal bovine serum (Wisent), 100 µg/ml streptomycin and 100 units/ml penicillin (Wisent). Cells were cultured at 37°C under a 5% CO_2 atmosphere.

STAU1-KO HCT116 cell lines

STAU1-KO HCT116 cells were generated by the CRISPR/Cas9 technology (Jinek et al., 2012). Briefly, HCT116 cells were transfected with plasmid coding for GFP, Cas9 and a single guide RNA targeting exon 6 of the *STAU1* gene (Horizon Discovery), using Lipofectamine 3000 (Life Technologies/Thermo Fisher). At 48 h post-transfection, GFP-positive cells were sorted by FACS and individual cells were grown on 96-well plates until colonies formed. Loss of STAU1 expression was monitored by western blotting using anti-STAU1 antibody. For growth curve assays, cells were harvested every day and the number of cells was counted with an automatic cell counter (TC20; Bio-Rad). The STAU1-KO clone CR1.3 was used in all experiments requiring STAU1 depletion. Clone CXR2.9 was used in the RT-qPCR experiment.

Cell lysates and immunoblotting

Cells were harvested in phosphate buffered saline (PBS) and lysed in Tris-SDS buffer [250 mM Tris-HCl pH 7.5, 15 mM EDTA, 0.5% Triton X-100, 5% (w/v) SDS, 100 mM NaCl and 1 mM dithiothreitol] supplemented with a cocktail of protease and phosphatase inhibitors (Sigma-Aldrich) for 10 min. Proteins were separated by SDS-PAGE and transferred to nitrocellulose membranes (Millipore). Membranes were blocked for 1 h in PBST (1× PBS, 0.05% Tween 20) containing 5% non-fat dry milk. Primary antibodies were prepared in 1% (w/v) skim milk in PBS-Tween 20 (0.2%) and 0.1% (w/v) sodium azide. Membranes were incubated at room temperature with antibodies for 1 or 16 h (anti-STAU2). Secondary antibodies were prepared in 2.5% (w/v) skim milk in PBS-Tween 20 (0.2%). Membranes were incubated at room temperature for 1 h with polyclonal goat anti-mouse (Dako) or anti-rabbit (Dako) HRP-conjugated secondary antibodies. Antibody-reactive bands were detected with chemiluminescence substrate ECL kit (GE Healthcare) using ChemiDoc MP Systems (Bio-Rad) or X-ray films (Fujifilm).

OP-puromycin

Active sites of translation were visualized with the Click-iT Plus OPP Protein Synthesis Assay Kit (Thermofisher) as recommended by the manufacturer. Briefly, cells were incubated with 20 µM Click-iT OP-puromycin solution for 30 min, fixed in 3.7% formaldehyde in PBS for 15 min and permeabilized in 0.5% Triton X-100 for 15 min. OP-puromycin was detected with Click-iT Plus OPP Reaction Cocktail. Images were acquired with an inverted Axio Observer Z1 confocal spinning disk microscope (Zeiss). Images was processed with the Zen Elite blue edition or ImageJ software.

Immunofluorescence microscopy

Cells were seeded onto poly-L-lysine-treated 20 mm coverslips in a six-well plate at 40% confluence and incubated overnight at 37°C. Cells were permeabilized in 150 mM NaCl, 10 mM Tris (pH 7.7), 0.5% Triton-X-100 (v/v) and 0.1% BSA (w/v) for 5 min and then fixed with 4% paraformaldehyde in PBS for 10 min at room temperature. Fixed cells were washed three times in PBS and blocked in PBS containing 0.1% BSA, 0.02% sodium azide and 1% goat serum for 1 h at room temperature. Cells were immuno-stained in blocking buffer containing antibodies for 16 h at 4°C. Secondary fluorochrome-conjugated antibodies (AlexaFluor 488 goat anti-mouse, AlexaFluor 488 goat anti-rabbit, AlexaFluor 568 goat anti-mouse, or AlexaFluor 568 goat anti-rabbit (Molecular Probes-Invitrogen) were added for 1 h at room temperature. Coverslips were washed and mounted on glass slides using ProLongTM Diamond Antifade mountant media (Thermofisher) containing 4′,6-diamidino-2-phenylindole (DAPI). Images were acquired with an inverted Axio Observer Z1 confocal spinning disk microscope (Zeiss). Image processing was performed using Zen Elite blue edition or ImageJ software.

Mitotic spindle preparation

Mitotic spindles were prepared from mitosis synchronized cells essentially as described (Blower et al., 2007). Briefly, mitotic cells were synchronized in late G2 with RO-3306, released and incubated in the presence of taxol (100 µM) for 15 min to stabilize polymerized microtubules. Mitotic cells were collected by shake-off and cell extracts were diluted in lysis buffer (100 mM PIPES pH 6.8, 1 mM $MgSO_4$, 2 mM EGTA, 4 µg/mL taxol, 2 µg/mL latrunculin B, 0.5% NP-40, 200 µg DNAse 1, 1 U/mL micrococcal nuclease, 20 U/mL benzonate, protease and phosphatase inhibitor cocktails) and centrifuged for 2 min at 700×***g***. The microtubule pellet was dissolved in hypotonic buffer (1 mM PIPES, 5 µg/mL taxol) and centrifuged again at 1500×***g*** for 3 min to obtain purified mitotic spindle. Micrococcal nuclease was omitted when spindle-associated RNAs were purified.

Genomic DNA sequencing

Genomic DNA was isolated (Bio Basic) and PCR-amplified using the Phusion polymerase (NEB) and specifics primers flanking exon 6 of the *STAU1* gene (sense, 5′-AGCCAAGTTTTTGTCTCAGCC-3′; antisense, 5′-ACAGCTGTCAATGTGCCTTCT-3′). PCR products were cloned into a pBluescript SK (+) vector (Stratagene). Ten clones were randomly chosen and sequenced (Genome Québec).

RNA extraction and real-time quantitative PCR

Total RNA was extracted using Trizol Reagent (Invitrogen) and reverse transcribed into cDNA using the RevertAid H Minus Reverse Transcriptase kit (Thermo Fisher Scientific). RNA was resuspended in 20 µL water and digested with DNaseI using the amplification grade AMPD1 kit (Sigma-Aldrich) prior to reverse transcription. Reverse transcription reactions were done with 1 µg RNA, MuLV RT enzyme and random hexamer (Thermo Fisher Scientific) according to the manufacturer's protocol. Resulting cDNAs were qPCR amplified using the Roche LightCycler 480 SYBR Green I Master kit and the LightCycler 480 instrument (Roche Applied Science). Cycling conditions were set at 95°C for 30 s, 60°C for 30 s and

72°C for 30 s, and 45 cycles. Sense and antisense primers were, respectively, ASPM, 5′-GCACCTTTCTGCCATTCTTGAGG-3′ and 5′-TGCTCCACTCTGGGCCATGT-3′; MEX3D, 5′-CAGATGAGCGTGATCGGCA-3′ and 5′-TGTTTGTCTTGGCCCGCAG-3′; FAM101B, 5′-GGCTTTGTCCCCTGTCCTTT-3′ and 5′-GCCTCTCGGAGTCGTACTTG-3′; NAT8L, 5′-CGCTACTACTACAGCCGCAAG-3′ and 5′-CACAATGCCCACCACGTTGC-3; HPRT, 5′-GCTTTCCTTGGTCAGGCAGT-3′ and 5′-CTTCGTGGGGTCCTTTTCACC-3′; RPL22, 5′-TGGTGACCATCGAAAGGAGCAAGA-3′ and 5′-TTGCTGTTAGCAACTACGCGCAAC-3′; ETS-18S, 5′-CGCCGCGCTCTACCTTACC-3′ and 5′-CGAGCGACCAAAGGAACCAT-3′; ITS1-5.8S, 5′-CTCGCCAAATCGACCTCGTA-3′ and 5′-GCAAGTGCGTTCGAAGTGTC-3′.

RNA-Seq and differential gene expression analysis

HCT116 were lysed in Trizol reagent (Life technologies) and RNA extracted. TURBO DNA-free Kit (Thermo Fisher Scientific) was used to eliminate DNA contamination, and RNA was purified using the RNeasy mini kit (Qiagen). Ribosomal RNA sequences were removed with the RiboMinus Eukaryote kit for RNA-Seq (ThermoFisher). RNA-Seq libraries were prepared using TruSeq stranded total RNA sample preparation kit (Illumina). Read quality was assessed using FastQC. No trimming was deemed necessary. Read alignment was executed using TopHat on the Human GRCh37 genomes from Ensembl (Trapnell et al., 2012). The GTF annotation file used during the alignment and for counting the number of reads aligned to each feature was also downloaded from Ensembl (release 75). Read count was obtained with featureCounts (Liao et al., 2014). Normalized count values (FPKM) and differential expression was computed with DESeq2 (Anders and Huber, 2010). Gene biotypes and additional information were obtained via the biomaRt R library (Durinck et al., 2009). All correlations and analysis were performed using R. The data discussed in this publication have been deposited in the NCBI Gene Expression Omnibus (Edgar et al., 2002) and are accessible through GEO Series accession number GSE138441 (https://www.ncbi.nlm.nih.gov/geo/query/acc.cgi?acc=GSE138441).

Acknowledgements

We thank Louise Cournoyer in the cell culture facility in the Département de biochimie et médecine moléculaire. We thank the molecular biology and functional genomics core facilities (Odile Neyret, Alexis Blanchet-Cohen) at the Institut de Recherches Cliniques de Montreal (IRCM) and the gene expression analysis core facilities at Genome Quebec Innovation Centre (McGill University) for transcriptomics approaches.

Competing interests

The authors declare no competing or financial interests.

Author contributions

Conceptualization: S.H., F.B.-M., L.P.B.B., M.G., L.D.; Methodology: S.H., F.B.-M., L.P.B.B., M.G.; Software: L.P.B.B., E.L.; Validation: F.B.-M., B.D., M.G., L.D.; Formal analysis: L.P.B.B.; Investigation: S.H., F.B.-M., L.P.B.B., B.D., M.G., M.B.; Data curation: L.P.B.B.; Writing - original draft: L.D.; Writing - review & editing: S.H., F.B.-M., L.P.B.B., B.D., M.G., M.B., E.L., L.D.; Visualization: S.H., F.B.-M., L.P.B.B., B.D., M.G., M.B., L.D.; Supervision: S.H., F.B.-M., E.L., L.D.; Project administration: E.L., L.D.; Funding acquisition: L.D.

Funding

This work was supported by a grant from the Canadian Institutes for Health Research (MOP-229979 to L.D.]; and the Bristol-Myers Squibb Canada chair in molecular biology to L.D.

Data availability

The data discussed in this publication have been deposited in the NCBI Gene Expression Omnibus (GEO) under accession number GSE138441.

Supplementary information

Supplementary information available online at
https://jcs.biologists.org/lookup/doi/10.1242/jcs.247155.supplemental

Peer review history

The peer review history is available online at
https://jcs.biologists.org/lookup/doi/10.1242/jcs.247155.reviewer-comments.pdf

References

Alliegro, M. C. and Alliegro, M. A. (2013). Localization of rRNA transcribed spacer domains in the nucleolinus and maternal procentrosomes of surf clam (Spisula) oocytes. *RNA Biol.* **10**, 391-396. doi:10.4161/rna.23548

Anders, S. and Huber, W. (2010). Differential expression analysis for sequence count data. *Genome Biol.* **11**, R106. doi:10.1186/gb-2010-11-10-r106

Aviner, R., Geiger, T. and Elroy-Stein, O. (2013). Novel proteomic approach (PUNCH-P) reveals cell cycle-specific fluctuations in mRNA translation. *Genes & Dev.* **27**, 1834-1844. doi:10.1101/gad.219105.113

Bélanger, G., Stocksley, M. A., Vandromme, M., Schaeffer, L., Furic, L., DesGroseillers, L. and Jasmin, B. J. (2003). Localization of the RNA-binding proteins Staufen1 and Staufen2 at the mammalian neuromuscular junction. *J. Neurochem.* **86**, 669-677. doi:10.1046/j.1471-4159.2003.01883.x

Blower, M. D., Feric, E., Weis, K. and Heald, R. (2007). Genome-wide analysis demonstrates conserved localization of messenger RNAs to mitotic microtubules. *J. Cell Biol.* **179**, 1365-1373. doi:10.1083/jcb.200705163

Bonner, M. K., Poole, D. S., Xu, T., Sarkeshik, A., Yates 3rd, J. R. and Skop, A. R. (2011). Mitotic spindle proteomics in Chinese hamster ovary cells. *PLoS One* **6**, e20489. doi:10.1371/journal.pone.0020489

Boulay, K., Ghram, M., Viranaicken, W., Trépanier, V., Mollet, S., Frechina, C. and DesGroseillers, L. (2014). Cell cycle-dependent regulation of the RNA-binding protein Staufen1. *Nucleic Acids Res.* **42**, 7867-7883. doi:10.1093/nar/gku506

Cao, Y., Du, J., Chen, D., Wang, Q., Zhang, N., Liu, X., Liu, X., Weng, J., Liang, Y. and Ma, W. (2016). RNA- binding protein Stau2 is important for spindle integrity and meiosis progression in mouse oocytes. *Cell Cycle* **15**, 2608-2618. doi:10.1080/15384101.2016.1208869

Carron, C., Balor, S., Delavoie, F., Plisson-Chastang, C., Faubladier, M., Gleizes, P. E. and O'Donohue, M. F. (2012). Post-mitotic dynamics of pre-nucleolar bodies is driven by pre-rRNA processing. *J. Cell Sci.* **125**, 4532-4542. doi:10.1242/jcs.106419

Chao, J. A., Yoon, Y. J. and Singer, R. H. (2012). Imaging translation in single cells using fluorescent microscopy. *Cold Spring Harb. Perspect. Biol.* **4**.

Chatel-Chaix, L., Boulay, K., Mouland, A. J. and Desgroseillers, L. (2008). The host protein Staufen1 interacts with the Pr55Gag zinc fingers and regulates HIV-1 assembly via its N-terminus. *Retrovirology* **5**, 41. doi:10.1186/1742-4690-5-41

Cho, H., Kim, K. M., Han, S., Choe, J., Park, S. G., Choi, S. S. and Kim, Y. K. (2012). Staufen1-mediated mRNA decay functions in adipogenesis. *Mol. Cell* **46**, 495-506. doi:10.1016/j.molcel.2012.03.009

Cummins, J. E., Blomquist, J. C. and Rusch, H. P. (1966). Anaphase delay after inhibition of protein synthesis between late prophase and prometaphase. *Science* **154**, 1343-1344. doi:10.1126/science.154.3754.1343

Damas, N. D., Marcatti, M., Come, C., Christensen, L. L., Nielsen, M. M., Baumgartner, R., Gylling, H. M., Maglieri, G., Rundsten, C. F., Seemann, S. E. et al. (2016). SNHG5 promotes colorectal cancer cell survival by counteracting STAU1-mediated mRNA destabilization. *Nat. Commun.* **7**, 13875. doi:10.1038/ncomms13875

de Lucas, S., Oliveros, J. C., Chagoyen, M. and Ortin, J. (2014). Functional signature for the recognition of specific target mRNAs by human Staufen1 protein. *Nucleic Acids Res.* **42**, 4516-4526. doi:10.1093/nar/gku073

Dionisio-Vicuna, M. N., Gutiérrez-López, T. Y., Adame-Garcia, S. R., Vázquez-Prado, J. and Reyes-Cruz, G. (2018). VPS28, an ESCRT-I protein, regulates mitotic spindle organization via Gbetagamma, EG5 and TPX2. *Biochim. Biophys. Acta Mol. Cell Res.* **1865**, 1012-1022. doi:10.1016/j.bbamcr.2018.03.005

Duchaine, T., Wang, H.-J., Luo, M., Steinberg, S. V., Nabi, I. R. and DesGroseillers, L. (2000). A novel murine Staufen isoform modulates the RNA content of Staufen complexes. *Mol. Cell. Biol.* **20**, 5592-5601. doi:10.1128/MCB.20.15.5592-5601.2000

Duchaine, T. F., Hemraj, I., Furic, L., Deitinghoff, A., Kiebler, M. A. and DesGroseillers, L. (2002). Staufen2 isoforms localize to the somatodendritic domain of neurons and interact with different organelles. *J. Cell Sci.* **115**, 3285-3295.

Dugre-Brisson, S., Elvira, G., Boulay, K., Chatel-Chaix, L., Mouland, A. J. and DesGroseillers, L. (2005). Interaction of Staufen1 with the 5′ end of mRNA facilitates translation of these RNAs. *Nucleic Acids Res.* **33**, 4797-4812. doi:10.1093/nar/gki794

Dundr, M., Misteli, T. and Olson, M. O. (2000). The dynamics of postmitotic reassembly of the nucleolus. *J. Cell Biol.* **150**, 433-446. doi:10.1083/jcb.150.3.433

Durinck, S., Spellman, P. T., Birney, E. and Huber, W. (2009). Mapping identifiers for the integration of genomic datasets with the R/Bioconductor package biomaRt. *Nat. Protoc.* **4**, 1184-1191. doi:10.1038/nprot.2009.97

Edgar, R., Domrachev, M. and Lash, A. E. (2002). Gene Expression Omnibus: NCBI gene expression and hybridization array data repository. *Nucleic Acids Res.* **30**, 207-210. doi:10.1093/nar/30.1.207

Elbarbary, R. A., Li, W., Tian, B. and Maquat, L. E. (2013). STAU1 binding 3′ UTR IRAlus complements nuclear retention to protect cells from PKR-mediated translational shutdown. *Genes Dev.* **27**, 1495-1510. doi:10.1101/gad.220962.113

Eliscovich, C., Peset, I., Vernos, I. and Mendez, R. (2008). Spindle-localized CPE-mediated translation controls meiotic chromosome segregation. *Nat. Cell Biol.* **10**, 858-865. doi:10.1038/ncb1746

Ferrandon, D., Elphick, L., Nusslein-Volhard, C. and St Johnston, D. (1994). Staufen protein associates with the 3′UTR of bicoid mRNA to form particles that move in a microtubule-dependent manner. *Cell* **79**, 1221-1232. doi:10.1016/0092-8674(94)90013-2

Furic, L., Maher-Laporte, M. and DesGroseillers, L. (2008). A genome-wide approach identifies distinct but overlapping subsets of cellular mRNAs associated with Staufen1- and Staufen2-containing ribonucleoprotein complexes. *RNA* **14**, 324-335. doi:10.1261/rna.720308

Gautrey, H., McConnell, J., Lako, M., Hall, J. and Hesketh, J. (2008). Staufen1 is expressed in preimplantation mouse embryos and is required for embryonic stem cell differentiation. *Biochim. Biophys. Acta* **1783**, 1935-1942. doi:10.1016/j.bbamcr.2008.05.017

Ghram, M., Bonnet-Magnaval, F., Hotea, D. I., Doran, B., Ly, S. and DesGroseillers, L. (2020). Staufen1 is essential for cell cycle transtions and cell proliferation via the control of E2F1 expression. *J. Mol. Biol.* **432**, 3881-3897. doi:10.1016/j.jmb.2020.04.016

Goetze, B., Tuebing, F., Xie, Y., Dorostkar, M. M., Thomas, S., Pehl, U., Boehm, S., Macchi, P. and Kiebler, M. A. (2006). The brain-specific double-stranded RNA-binding protein Staufen2 is required for dendritic spine morphogenesis. *J. Cell Biol.* **172**, 221-231. doi:10.1083/jcb.200509035

Gong, C., Kim, Y. K., Woeller, C. F., Tang, Y. and Maquat, L. E. (2009). SMD and NMD are competitive pathways that contribute to myogenesis: effects on PAX3 and myogenin mRNAs. *Genes Dev.* **23**, 54-66. doi:10.1101/gad.1717309

Groisman, I., Huang, Y. S., Mendez, R., Cao, Q., Theurkauf, W. and Richter, J. D. (2000). CPEB, maskin, and cyclin B1 mRNA at the mitotic apparatus: implications for local translational control of cell division. *Cell* **103**, 435-447. doi:10.1016/S0092-8674(00)00135-5

Heber, S., Gáspár, I., Tants, J. N., Gunther, J., Moya, S. M. F., Janowski, R., Ephrussi, A., Sattler, M. and Niessing, D. (2019). Staufen2-mediated RNA recognition and localization requires combinatorial action of multiple domains. *Nat. Commun.* **10**, 1659. doi:10.1038/s41467-019-09655-3

Hernandez-Verdun, D. (2011). Assembly and disassembly of the nucleolus during the cell cycle. *Nucleus* **2**, 189-194. doi:10.4161/nucl.2.3.16246

Hornbeck, P. V., Zhang, B., Murray, B., Kornhauser, J. M., Latham, V. and Skrzypek, E. (2015). PhosphoSitePlus, 2014: mutations, PTMs and recalibrations. *Nucleic Acids Res.* **43**, D512-D520. doi:10.1093/nar/gku1267

Hussain, S., Benavente, S. B., Nascimento, E., Dragoni, I., Kurowski, A., Gillich, A., Humphreys, P. and Frye, M. (2009). The nucleolar RNA methyltransferase Misu (NSun2) is required for mitotic spindle stability. *J. Cell Biol.* **186**, 27-40. doi:10.1083/jcb.200810180

Jeong, K., Ryu, I., Park, J., Hwang, H. J., Ha, H., Park, Y., Oh, S. T. and Kim, Y. K. (2019). Staufen1 and UPF1 exert opposite actions on the replacement of the nuclear cap-binding complex by eIF4E at the 5′ end of mRNAs. *Nucleic Acids Res.* **47**, 9313-9328. doi:10.1093/nar/gkz643

Jinek, M., Chylinski, K., Fonfara, I., Hauer, M., Doudna, J. A. and Charpentier, E. (2012). A programmable dual-RNA-guided DNA endonuclease in adaptive bacterial immunity. *Science* **337**, 816-821. doi:10.1126/science.1225829

Keene, J. D. (2007). RNA regulons: coordination of post-transcriptional events. *Nat. Rev. Genet.* **8**, 533-543. doi:10.1038/nrg2111

Khatua, S., Peterson, K. M., Brown, K. M., Lawlor, C., Santi, M. R., LaFleur, B., Dressman, D., Stephan, D. A. and MacDonald, T. J. (2003). Overexpression of the EGFR/FKBP12/HIF-2alpha pathway identified in childhood astrocytomas by angiogenesis gene profiling. *Cancer Res.* **63**, 1865-1870.

Kiebler, M. A., Hemraj, I., Verkade, P., Kohrmann, M., Fortes, P., Marión, R. M., Ortin, J. and Dotti, C. G. (1999). The mammalian staufen protein localizes to the somatodendritic domain of cultured hippocampal neurons: implications for its involvement in mRNA transport. *J. Neurosci.* **19**, 288-297. doi:10.1523/JNEUROSCI.19-01-00288.1999

Kim, Y. K., Furic, L., DesGroseillers, L. and Maquat, L. E. (2005). Mammalian Staufen1 recruits Upf1 to specific mRNA 3'UTRs so as to elicit mRNA decay. *Cell* **120**, 195-208. doi:10.1016/j.cell.2004.11.050

Kim, Y. K., Furic, L., Parisien, M., Major, F., DesGroseillers, L. and Maquat, L. E. (2007). Staufen1 regulates diverse classes of mammalian transcripts. *EMBO J.* **26**, 2670-2681. doi:10.1038/sj.emboj.7601712

Kingsley, E. P., Chan, X. Y., Duan, Y. and Lambert, J. D. (2007). Widespread RNA segregation in a spiralian embryo. *Evol. Dev.* **9**, 527-539. doi:10.1111/j.1525-142X.2007.00194.x

Kretz, M. (2013). TINCR, staufen1, and cellular differentiation. *RNA Biol.* **10**, 1597-1601. doi:10.4161/rna.26249

Laver, J. D., Li, X., Ancevicius, K., Westwood, J. T., Smibert, C. A., Morris, Q. D. and Lipshitz, H. D. (2013). Genome-wide analysis of Staufen-associated mRNAs identifies secondary structures that confer target specificity. *Nucleic Acids Res.* **41**, 9438-9460. doi:10.1093/nar/gkt702

Lebeau, G., Maher-Laporte, M., Topolnik, L., Laurent, C. E., Sossin, W., Desgroseillers, L. and Lacaille, J. C. (2008). Staufen1 regulation of protein synthesis-dependent long-term potentiation and synaptic function in hippocampal pyramidal cells. *Mol. Cell. Biol.* **28**, 2896-2907. doi:10.1128/MCB.01844-07

Lebeau, G., Miller, L. C., Tartas, M., McAdam, R., Laplante, I., Badeaux, F., DesGroseillers, L., Sossin, W. S. and Lacaille, J. C. (2011). Staufen 2 regulates mGluR long-term depression and Map1b mRNA distribution in hippocampal neurons. *Learn. Mem.* **18**, 314-326. doi:10.1101/lm.2100611

LeGendre, J. B., Campbell, Z. T., Kroll-Conner, P., Anderson, P., Kimble, J. and Wickens, M. (2013). RNA targets and specificity of Staufen, a double-stranded RNA-binding protein in Caenorhabditis elegans. *J. Biol. Chem.* **288**, 2532-2545. doi:10.1074/jbc.M112.397349

Liao, Y., Smyth, G. K. and Shi, W. (2014). featureCounts: an efficient general purpose program for assigning sequence reads to genomic features. *Bioinformatics* **30**, 923-930. doi:10.1093/bioinformatics/btt656

Liu, Z., Chen, Z., Fan, R., Jiang, B., Chen, X., Chen, Q., Nie, F., Lu, K. and Sun, M. (2017). Over-expressed long noncoding RNA HOXA11-AS promotes cell cycle progression and metastasis in gastric cancer. *Mol. Cancer* **16**, 82. doi:10.1186/s12943-017-0651-6

Luo, M., Duchaine, T. F. and DesGroseillers, L. (2002). Molecular mapping of the determinants involved in human Staufen-ribosome association. *Biochem. J.* **365**, 817-824. doi:10.1042/bj20020263

Marión, R. M., Fortes, P., Beloso, A., Dotti, C. and Ortin, J. (1999). A human sequence homologue of Staufen is an RNA-binding protein that is associated with polysomes and localizes to the rough endoplasmic reticulum. *Mol. Cell. Biol.* **19**, 2212-2219. doi:10.1128/MCB.19.3.2212

Martel, C., Macchi, P., Furic, L., Kiebler, M. A. and Desgroseillers, L. (2006). Staufen1 is imported into the nucleolus via a bipartite nuclear localization signal and several modulatory determinants. *Biochem. J.* **393**, 245-254. doi:10.1042/BJ20050694

Martel, C., Dugre-Brisson, S., Boulay, K., Breton, B., Lapointe, G., Armando, S., Trepanier, V., Duchaine, T., Bouvier, M. and Desgroseillers, L. (2010). Multimerization of Staufen1 in live cells. *RNA* **16**, 585-597. doi:10.1261/rna.1664210

Mayya, V. K. and Duchaine, T. F. (2019). Ciphers and Executioners: How 3′-Untranslated Regions Determine the Fate of Messenger RNAs. *Front. Genet.* **10**, 6. doi:10.3389/fgene.2019.00006

Micklem, D. R., Adams, J., Grunert, S. and St Johnston, D. (2000). Distinct roles of two conserved Staufen domains in oskar mRNA localization and translation. *EMBO J.* **19**, 1366-1377. doi:10.1093/emboj/19.6.1366

Morita, E., Colf, L. A., Karren, M. A., Sandrin, V., Rodesch, C. K. and Sundquist, W. I. (2010). Human ESCRT-III and VPS4 proteins are required for centrosome and spindle maintenance. *Proc. Natl Acad. Sci. USA* **107**, 12889-12894. doi:10.1073/pnas.1005938107

Neriec, N. and Percipalle, P. (2018). Sorting mRNA Molecules for Cytoplasmic Transport and Localization. *Front. Genet.* **9**, 510. doi:10.3389/fgene.2018.00510

Park, J.-E., Yi, H., Kim, Y., Chang, H. and Kim, V. N. (2016). Regulation of Poly(A) Tail and Translation during the Somatic Cell Cycle. *Mol. Cell* **62**, 462-471. doi:10.1016/j.molcel.2016.04.007

Petsalaki, E. and Zachos, G. (2018). Novel ESCRT functions at kinetochores. *Aging* **10**, 299-300. doi:10.18632/aging.101399

Petsalaki, E., Dandoulaki, M. and Zachos, G. (2018). The ESCRT protein Chmp4c regulates mitotic spindle checkpoint signaling. *J. Cell Biol.* **217**, 861-876. doi:10.1083/jcb.201709005

Rao, S. R., Flores-Rodriguez, N., Page, S. L., Wong, C., Robinson, P. J. and Chircop, M. (2016). The Clathrin-dependent Spindle Proteome. *Mol. Cell. Proteomics* **15**, 2537-2553. doi:10.1074/mcp.M115.054809

Rao, S., Hassine, S., Monette, A., Amorim, R., DesGroseillers, L. and Mouland, A. J. (2019). HIV-1 requires Staufen1 to dissociate stress granules and to produce infectious viral particles. *RNA* **25**, 727-736. doi:10.1261/rna.069351.118

Ravel-Chapuis, A., Bélanger, G., Yadava, R. S., Mahadevan, M. S., DesGroseillers, L., Côté, J. and Jasmin, B. J. (2012). The RNA-binding protein Staufen1 is increased in DM1 skeletal muscle and promotes alternative pre-mRNA splicing. *J. Cell Biol.* **196**, 699-712. doi:10.1083/jcb.201108113

Ricci, E. P., Kucukural, A., Cenik, C., Mercier, B. C., Singh, G., Heyer, E. E., Ashar-Patel, A., Peng, L. and Moore, M. J. (2014). Staufen1 senses overall transcript secondary structure to regulate translation. *Nat. Struct. Mol. Biol.* **21**, 26-35. doi:10.1038/nsmb.2739

Sakurai, M., Shiromoto, Y., Ota, H., Song, C. Z., Kossenkov, A. V., Wickramasinghe, J., Showe, L. C., Skordalakes, E., Tang, H.-Y., Speicher, D. W. et al. (2017). ADAR1 controls apoptosis of stressed cells by inhibiting Staufen1-mediated mRNA decay. *Nat. Struct. Mol. Biol.* **24**, 534-543. doi:10.1038/nsmb.3403

Sepulveda, G., Antkowiak, M., Brust-Mascher, I., Mahe, K., Ou, T., Castro, N. M., Christensen, L. N., Cheung, L., Jiang, X., Yoon, D. et al. (2018). Co-translational protein targeting facilitates centrosomal recruitment of PCNT during centrosome maturation in vertebrates. *Elife* **7**.

Sharp, J. A., Plant, J. J., Ohsumi, T. K., Borowsky, M. and Blower, M. D. (2011). Functional analysis of the microtubule-interacting transcriptome. *Mol. Biol. Cell* **22**, 4312-4323. doi:10.1091/mbc.e11-07-0629

Shishova, K. V., Zharskaya, C. O. and Zatsepina, C. O. (2011). The Fate of the Nucleolus during Mitosis: Comparative Analysis of Localization of Some Forms of Pre-rRNA by Fluorescent in Situ Hybridization in NIH/3T3 Mouse Fibroblasts. *Acta Naturae* **3**, 100-106. doi:10.32607/20758251-2011-3-4-100-106

Sirri, V., Jourdan, N., Hernandez-Verdun, D. and Roussel, P. (2016). Sharing of mitotic pre-ribosomal particles between daughter cells. *J. Cell Sci.* **129**, 1592-1604. doi:10.1242/jcs.180521

Stumpf, C. R., Moreno, M. V., Olshen, A. B., Taylor, B. S. and Ruggero, D. (2013). The Translational Landscape of the Mammalian Cell Cycle. *Mol. Cell* **52**, 574-582. doi:10.1016/j.molcel.2013.09.018

Sugimoto, Y., Vigilante, A., Darbo, E., Zirra, A., Militti, C., D'Ambrogio, A., Luscombe, N. M. and Ule, J. (2015). hiCLIP reveals the in vivo atlas of mRNA secondary structures recognized by Staufen 1. *Nature* **519**, 491-494. doi:10.1038/nature14280

Suter, B. (2018). RNA localization and transport. *Biochim. Biophys. Acta Gene Regul. Mech.* **1861**, 938-951. doi:10.1016/j.bbagrm.2018.08.004

Tanenbaum, M. E., Stern-Ginossar, N., Weissman, J. S. and Vale, R. D. (2015). Regulation of mRNA translation during mitosis. *Elife* **4**.

Thomas, M. G., Tosar, L. J., Desbats, M. A., Leishman, C. C. and Boccaccio, G. L. (2009). Mammalian Staufen 1 is recruited to stress granules and impairs their assembly. *J. Cell Sci.* **122**, 563-573. doi:10.1242/jcs.038208

Trapnell, C., Roberts, A., Goff, L., Pertea, G., Kim, D., Kelley, D. R., Pimentel, H., Salzberg, S. L., Rinn, J. L. and Pachter, L. (2012). Differential gene and transcript expression analysis of RNA-seq experiments with TopHat and Cufflinks. *Nat. Protoc.* **7**, 562-578. doi:10.1038/nprot.2012.016

Tripathi, S., Pohl, M. O., Zhou, Y. Y., Rodriguez-Frandsen, A., Wang, G. J., Stein, D. A., Moulton, H. M., DeJesus, P., Che, J. W., Mulder, L. C. F. et al. (2015). Meta- and orthogonal integration of influenza "OMICs'' data defines a role for UBR4 in virus budding. *Cell Host Microbe* **18**, 723-735. doi:10.1016/j.chom.2015.11.002

Van Nostrand, E. L., Pratt, G. A., Yee, B. A., Wheeler, E., Blue, S. M., Mueller, J., Park, S. S., Garcia, K. E., Gelboin-Burkhart, C., Nguyen, T. B. et al. (2020). Principles of RNA processing from analysis of enhanced CLIP maps for 150 RNA binding proteins. *Genome Biol.* **21**, 90. doi:10.1186/s13059-020-01982-9.

Vessey, J. P., Macchi, P., Stein, J. M., Mikl, M., Hawker, K. N., Vogelsang, P., Wieczorek, K., Vendra, G., Riefler, J., Tubing, F. et al. (2008). A loss of function allele for murine Staufen1 leads to impairment of dendritic Staufen1-RNP delivery and dendritic spine morphogenesis. *Proc. Natl Acad. Sci. USA* **105**, 16374-16379. doi:10.1073/pnas.0804583105

Vietri, M., Schink, K. O., Campsteijn, C., Wegner, C. S., Schultz, S. W., Christ, L., Thoresen, S. B., Brech, A., Raiborg, C. and Stenmark, H. (2015). Spastin and ESCRT-III coordinate mitotic spindle disassembly and nuclear envelope sealing. *Nature* **522**, 231-235. doi:10.1038/nature14408

Wan, D., Gong, Y., Qin, W., Zhang, P., Li, J., Wei, L., Zhou, X., Li, H., Qiu, X., Zhong, F. et al. (2004). Large-scale cDNA transfection screening for genes related to cancer development and progression. *Proc. Natl Acad. Sci. USA* **101**, 15724-15729. doi:10.1073/pnas.0404089101

Wickham, L., Duchaine, T., Luo, M., Nabi, I. R. and DesGroseillers, L. (1999). Mammalian staufen is a double-stranded-RNA- and tubulin-binding protein which localizes to the rough endoplasmic reticulum. *Mol. Cell. Biol.* **19**, 2220-2230. doi:10.1128/MCB.19.3.2220

Wilker, E. W., van Vugt, M. A., Artim, S. A., Huang, P. H., Petersen, C. P., Reinhardt, H. C., Feng, Y., Sharp, P. A., Sonenberg, N., White, F. M. et al. (2007). 14-3-3sigma controls mitotic translation to facilitate cytokinesis. *Nature* **446**, 329-332. doi:10.1038/nature05584

Xu, T. P., Liu, X. X., Xia, R., Yin, L., Kong, R., Chen, W. M., Huang, M. D. and Shu, Y. Q. (2015). SP1-induced upregulation of the long noncoding RNA TINCR regulates cell proliferation and apoptosis by affecting KLF2 mRNA stability in gastric cancer. *Oncogene* **34**, 5648-5661. doi:10.1038/onc.2015.18

Xu, T. P., Wang, Y. F., Xiong, W. L., Ma, P., Wang, W. Y., Chen, W. M., Huang, M. D., Xia, R., Wang, R., Zhang, E. B. et al. (2017). E2F1 induces TINCR transcriptional activity and accelerates gastric cancer progression via activation of TINCR/STAU1/CDKN2B signaling axis. *Cell Death Dis.* **8**, e2837. doi:10.1038/cddis.2017.205

Yamaguchi, Y., Oohinata, R., Naiki, T. and Irie, K. (2008). Stau1 negatively regulates myogenic differentiation in C2C12 cells. *Genes Cells* **13**, 583-592. doi:10.1111/j.1365-2443.2008.01189.x

SUPPLEMENTAL TABLES

Table S1. RNA-Seq of whole cell (Input) and spindle preparations (MS) isolated from WT (HCT) and STAU1-KO (CR1_3) cells

Click here to Download Table S1

Table S2. List of genes that are misregulated in STAU1-KO compared to wild-type HCT116 cells (Input)

Click here to Download Table S2

Table S3. Spindle-enriched RNAs in WT and STAU1-KO HCT116 cells

Click here to Download Table S3

Table S4. Number of individual transcripts and of transcripts per million (TPM) across RNA biotypes of spindle-enriched RNAs. Enrichment of TPM in mitotic spindle compared to input is shown.

Click here to Download Table S4

Table S5. Gene ontology (GO) of spindle-enriched RNAs in HCT116 cells (Metascape Gene Annotation & Analysis Resource).

Click here to Download Table S5

Table S6. Downregulated RNAs in spindle preparations of STAU1-KO cells compared to WT cells.

Click here to Download Table S6

Table S7. Gene ontology (GO) of downregulated RNAs in spindle preparations of STAU1-KO cells compared to WT cells (Metascape Gene Annotation & Analysis Resource).

Click here to Download Table S7

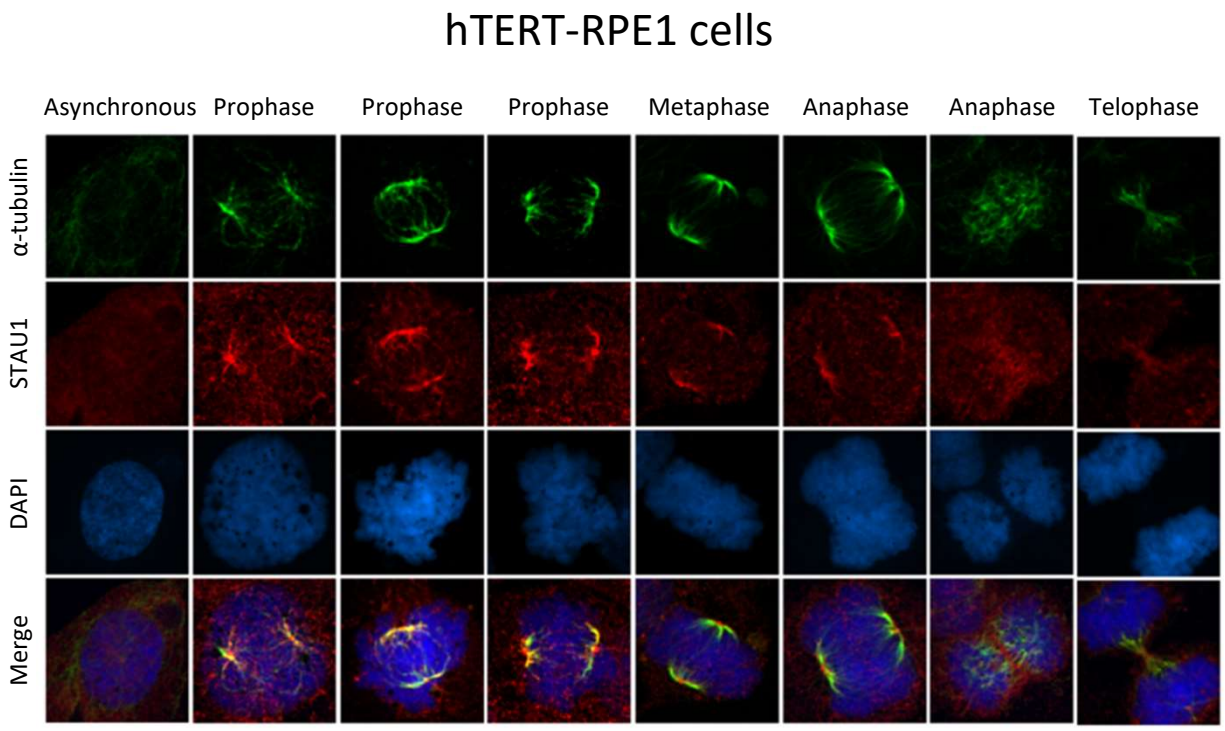

Figure S1. Co-localisation of STAU1 and α-tubulin on mitotic spindle in the non-transformed hTERT-RPE1 cells. hTERT-RPE1 cells were synchronized in late G_2 with RO-3306 and released from the block with fresh medium to reach mitosis. Cells were treated with Triton X-100 and then fixed. Proteins were stained with specific antibodies to detect Stau1 and α-tubulin. DNA was stained with DAPI. Cells at different steps of mitosis are shown.

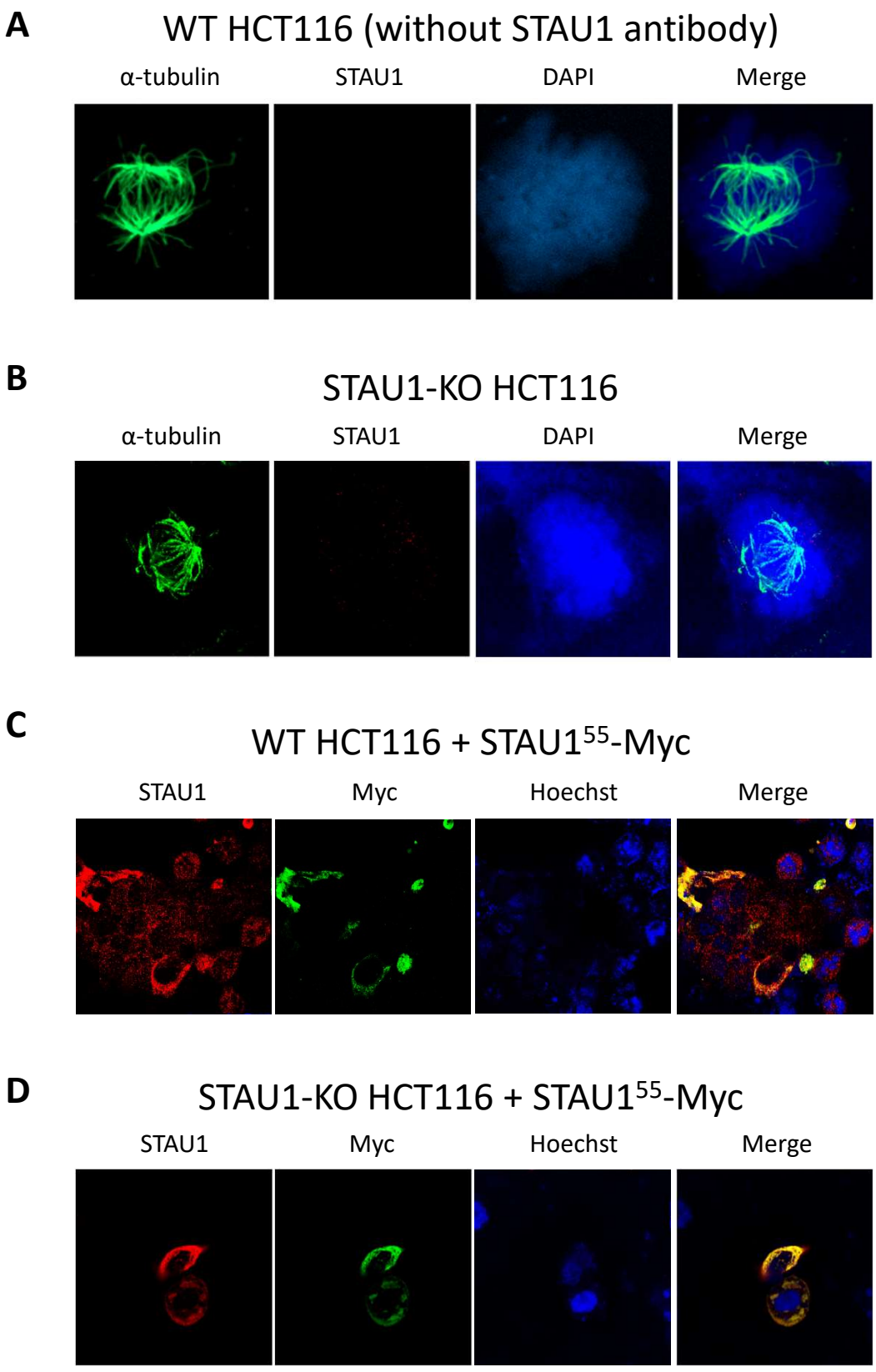

Figure S2. Control of antibody specificity. (A) To control for antibody specificity, mitotic HCT116 cells were stained with rabbit anti-tubulin antibody and anti-mouse (usually used to detect STAU1 expression) and anti-rabbit secondary antibodies. In the absence of anti-STAU1 antibody, no signal was detected. **(B)** STAU1-KO HCT116 cells (clone CR1.3) were stained with anti-STAU1 and anti-tubulin antibodies. No signal was detected with anti-STAU1 antibody. **(C,D)** HCT116 (C) and HCT116-KO (clone CR1.3) (D) cells were transfected with a plasmid coding for STAU1^{55}-myc and stained with anti-STAU1 and anti-myc antibodies. Perfect colocalization of STAU1 and myc signals are observed. These experiments are representative of at least three independently performed experiments.

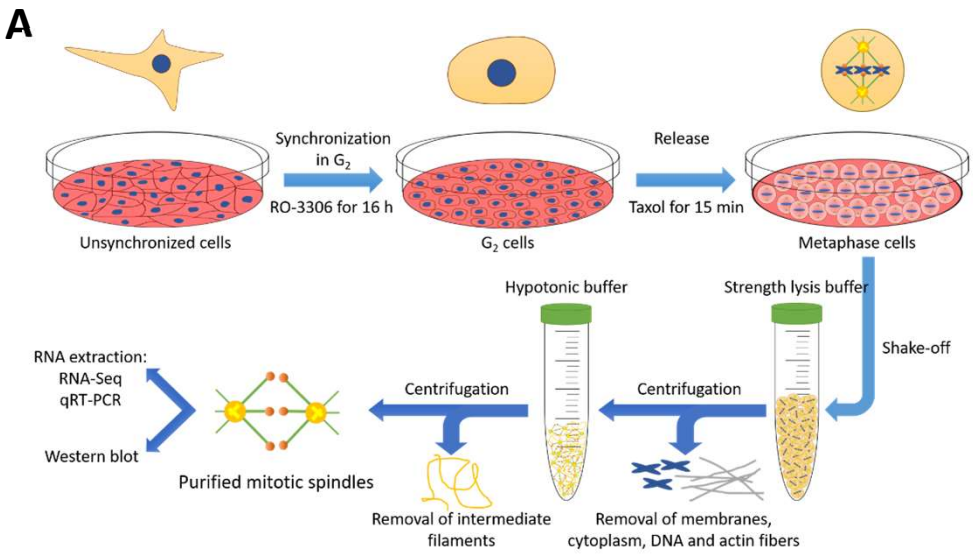

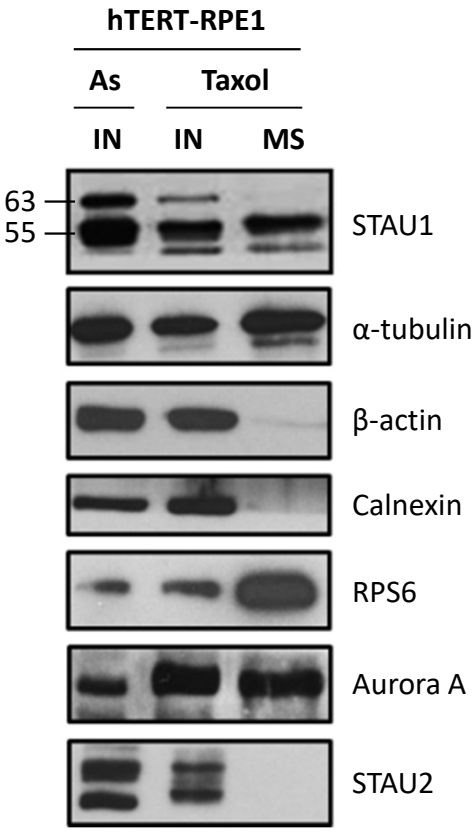

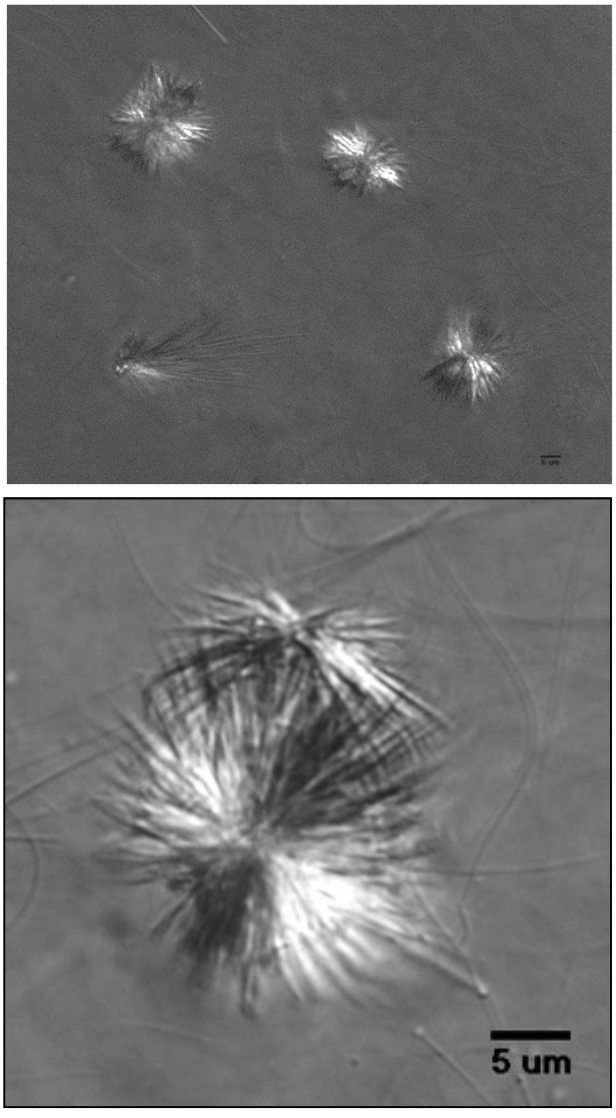

Figure S3. Validation of spindle preparations by microscopy. A) Schematic illustration of the protocol used to purify mitotic spindles. **B)** hTERT-RPE1 cells were synchronized in prometaphase and treated with taxol to stabilize microtubules. Mitotic spindles were purified and protein contents analyzed by western blotting. As, asynchronous cells; Taxol, mitotic cells; IN, input total cell extracts. MS: mitotic spindle. (n=3). **C)** Aliquots of spindle preparations were spread on microscopic slides and visualized by microscopy.

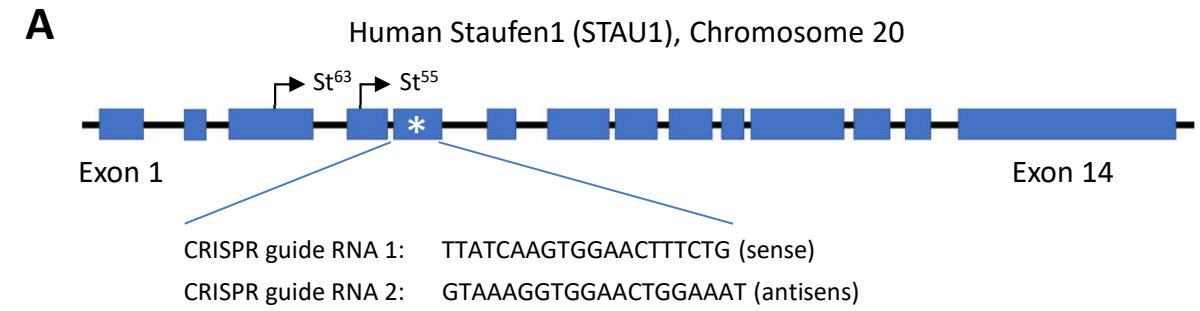

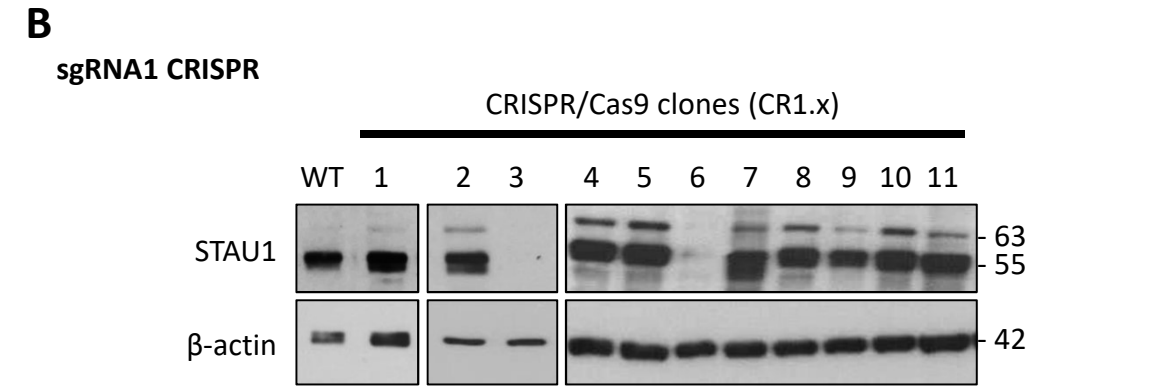

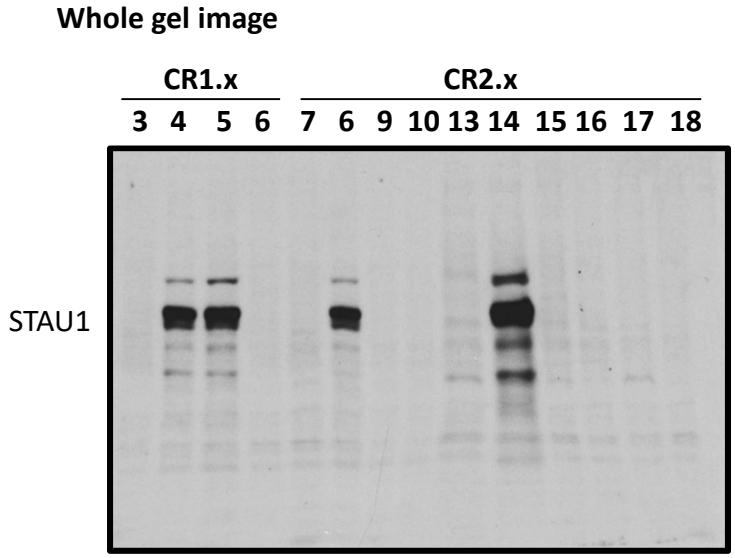

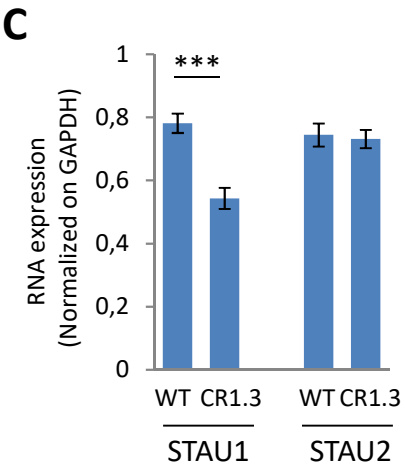

D

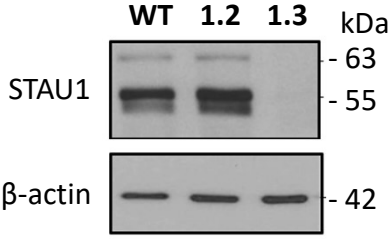

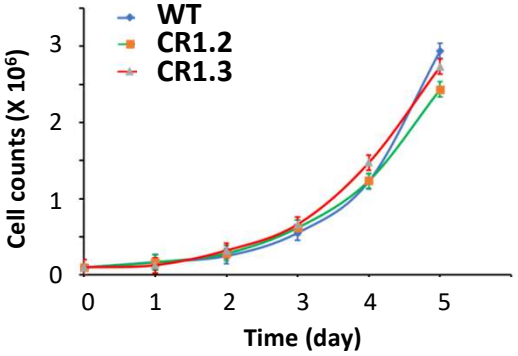

E

WT sequence:

sgRNA1 target sequence

```
TACTTTTACCCATTTCCAGTTCCACCTTTACTTTATCAAGTGGAACTTTCTGTGGGAGGACAGCAATTTAA
 Y  F  Y  P  F  P  V  P  P  L  L  Y  Q  V  E  L  S  V  G  G  Q  Q  F  N
```

CR1.3 - Allele 1:

```
TACTTTTACCCATTTCCAGTTCCACCTTTACTTTATCAAGTGGAACTTT--------GGACAGCAATTTAA
 Y  F  Y  P  F  P  V  P  P  L  L  Y  Q  V  E  L           W  T  A  I  Stop
```

CR1.3 - Allele 2:

```
TACTTTTACCCATTTCCAGTTCCACCTTTACTTTATCAAGTGGAAC---AGAAAGGCGGACAGGTATCCGG
 Y  F  Y  P  F  P  V  P  P  L  L  Y  Q  V  E     Q  K  G  G  Q  V  S  G

TAAGCGGCAGGGTCGGAACAGGAGAGCGCACGAGGGAGCTTCCAGGGGGAAACGCCTGGTATCTTTATAGT
  K  R  Q  G  R  N  R  R  A  H  E  G  A  S  R  G  K  R  L  V  S  L  Stop

CCTGTCGGGTTTCGCCACCTCTGACTTGAGCGTCGATTTTTGTGATGCTCGTCAGGGGGGCGGAGCCTATG
GAAAAACGCCAGCTGTGGGAGGACAGCAATTTAA
```

F

WT sequence:

sgRNA2 target sequence

```
TACTTTTACCCATTTCCAGTTCCACCTTTACTTTATCAAGTGGAACTTTCTGTGGGAGGACAGCAATTTAA
 Y  F  Y  P  F  P  V  P  P  L  L  Y  Q  V  E  L  S  V  G  G  Q  Q  F  N
```

CR2.9 - Allele 1:

```
TACTTTTACCCATTCTCCAGTTCCACCTTTACTTTATCAAGTGGAACTTTCTGTGGGAGGACAGCAATTTAA
 Y  F  Y  P  F  S  S  S  T  F  T  L  S  S  G  T  F  C  G  R  T  A  I  Stop
```

CR2.9 - Allele 2:

```
TACTTTTACCCATTTTCCAGTTCCACCTTTACTTTATCAAGTGGAACTTTCTGTGGGAGGACAGCAATTTAA
 Y  F  Y  P  F  S  S  S  T  F  T  L  S  S  G  T  F  C  G  R  T  A  I  Stop
```

Figure S4. Knockout of STAU1 in the colorectal HCT116 cancer cell line by the CRISPR/Cas9 complex system. (A) Schematic representation of the *STAU1* gene. Position of ATG initiation codons for STAU1 55 kDa and 63 kDa is indicated. * : site of CRISPR editing. Two different CRISPR guide RNAs were used. **(B)** HCT116 cells were transfected with plasmids expressing Cas9/sgRNA1 or Cas9/sgRNA2 complex targeting exon 6 of the *STAU1* gene. Colonies grown from single cell were screened for STAU1 expression by western blotting. 18% and 44% of the clones that were transfected with CRISPR sgRNA1 and CRISPR sgRNA2, respectively, were negative for STAU1 expression. Below, whole gel image of CR2.13 to CR2.18 cell extracts showing that STAU1-truncated products are not produced in CRISPR STAU1-KO cells. **(C)** Wild type (WT) and STAU1-KO (clone CR1.3) HCT116 cells were analyzed by RT-qPCR for STAU1 and STAU2 expression. **D)** Cells were plated at the same density and counted every day for five days. The graph shows the means and standard deviation of cell counts of three independently performed experiments**. E,F)** Biallelic sequencing of exon 6 of *STAU1* genomic DNA isolated from STAU1-KO CR1.3 (D) and CR2.9 (E) cells. Sequences of wild type (WT) and CRISPR alleles are shown as well as the corresponding protein sequence. The WT protein sequence is underlined. Red: Target sequences of the CRISPR sgRNA1. Green: Inserted nucleotides. Dash line: Deleted nucleotides

Supplementary Figure S5

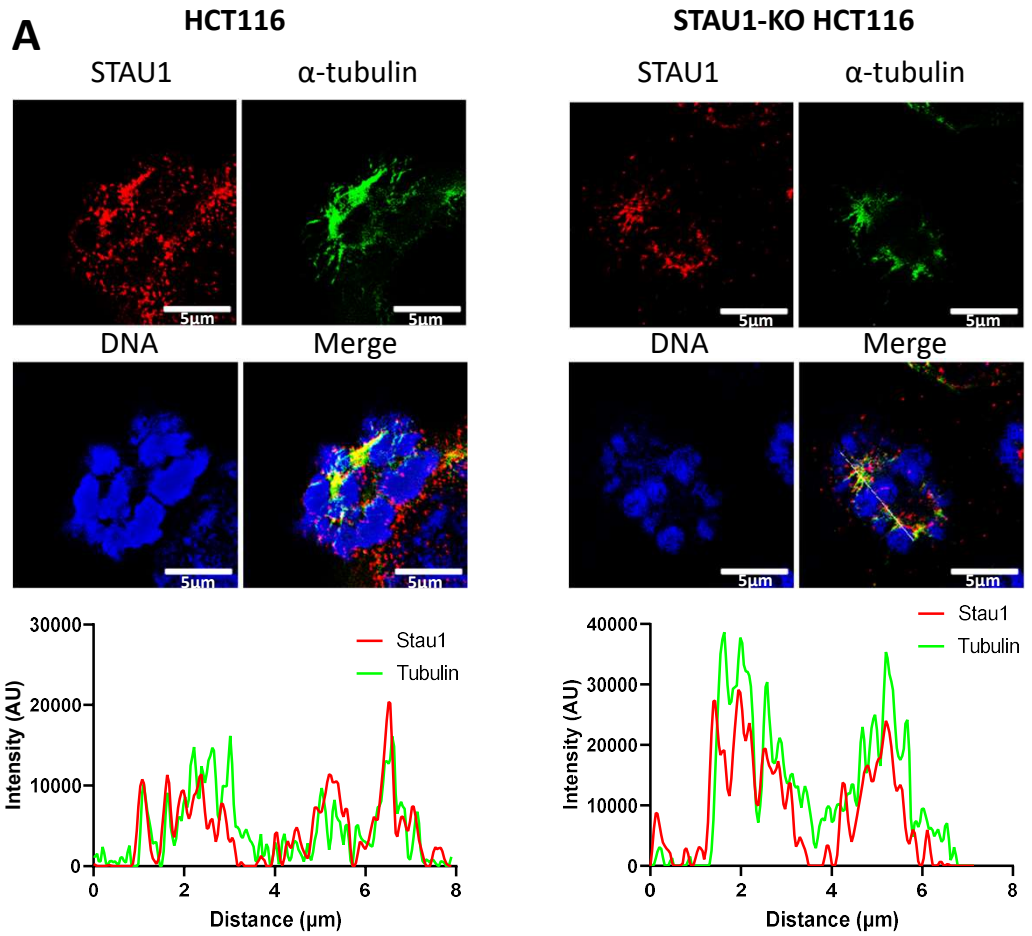

Figure S5. Characterization of exogenously expressed STAU1^{55}. A) HCT116 WT (left) and STAU1-KO CR1.3 (right) cells were transfected with a plasmid coding for STAU1^{55}-myc. STAU1 was detected with anti-STAU1 and anti-myc antibodies. Both signals co-localized as expected. **B)** Exogenously transfected STAU1^{55}-HA$_3$ purifies in mitotic spindle preparations, as does the endogenous protein. Western blot experiment showing endogenous STAU1 in cell extracts (IN) and spindle preparations (MS) of HCT116 cells (WT) and STAU1-HA$_3$ in cell extracts (IN) and spindle preparations (MS) of STAU1-KO HCT116 cells.

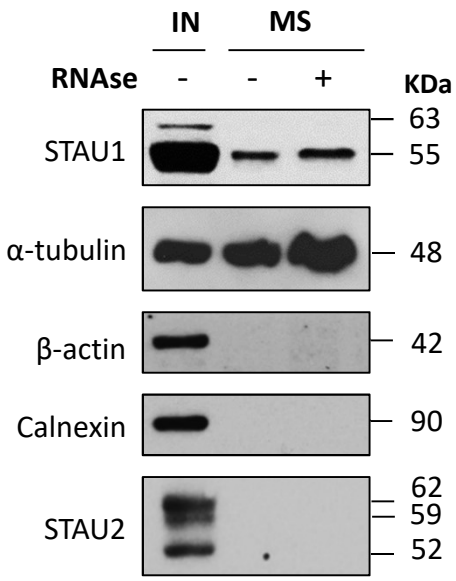

Figure S6. STAU1 association with spindle is resistant to RNase treatment. Western blot experiment of cell extracts (IN) and mitotic spindle preparations (MS) purified in the presence (+) or absence (-) of RNase.

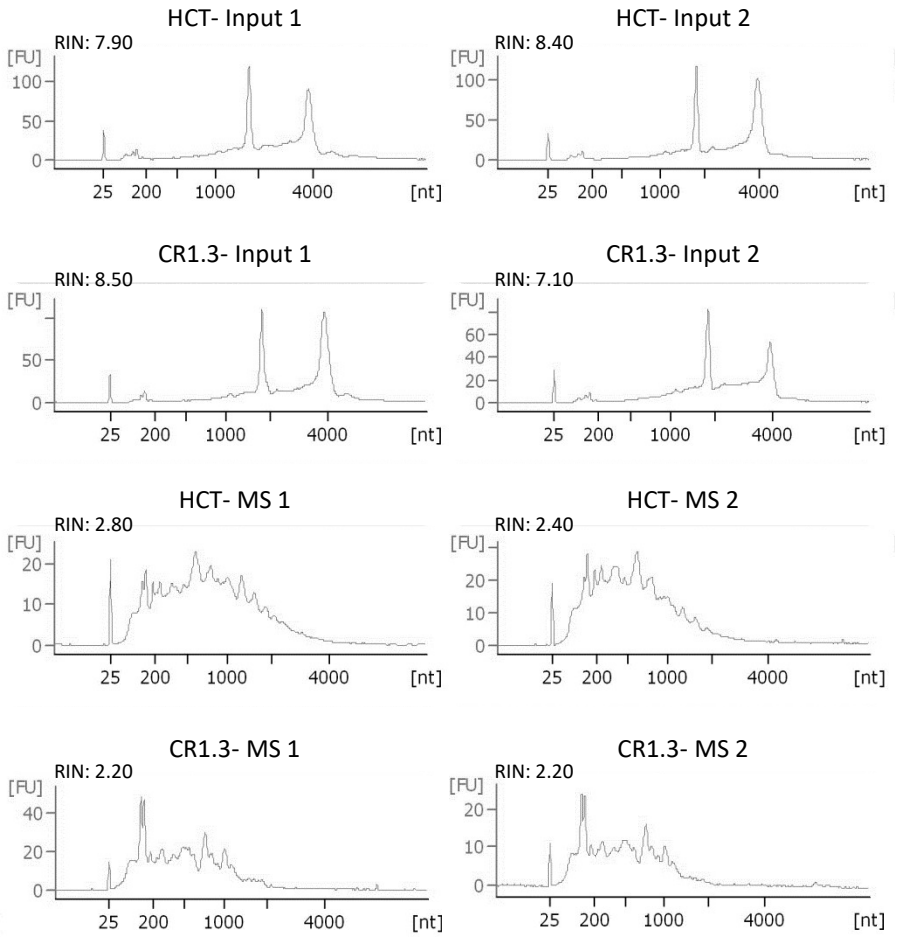

Figure S7. Quality controls of RNA-Seq data. RNAs were isolated from WT (HCT) and STAU1-KO (CR1.3) HCT116 cells and analyzed by Agilent RNA Pico. RNAs from total cell extracts (Input) and mitotic spindle preparations (MS) are shown.

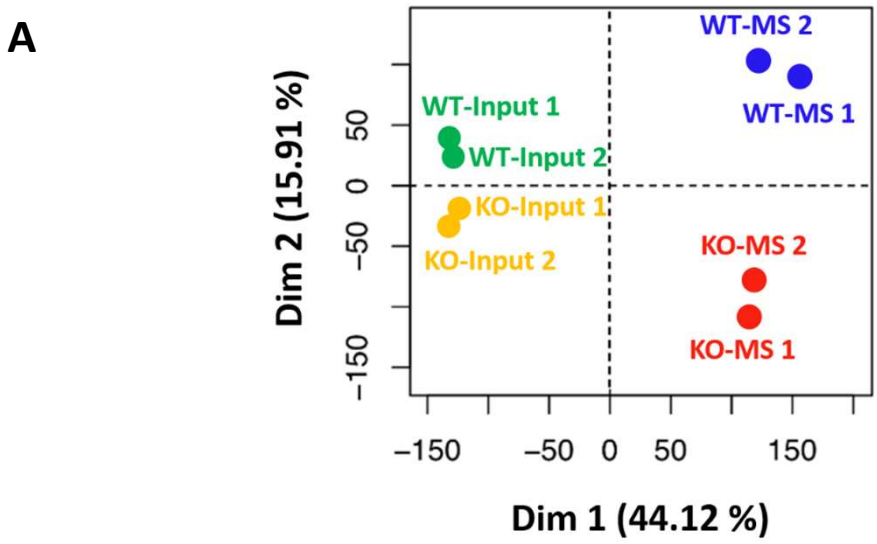

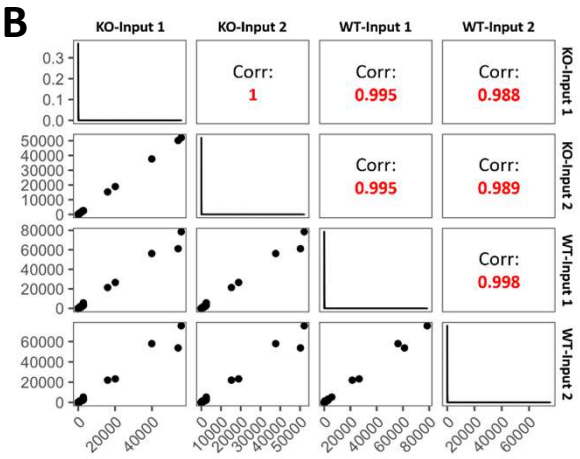

Correlations Input (WT vs STAU1-KO)

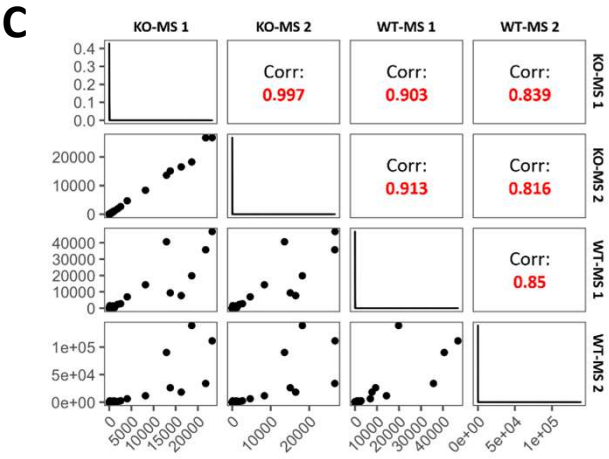

Correlations MS (WT vs STAU1-KO)

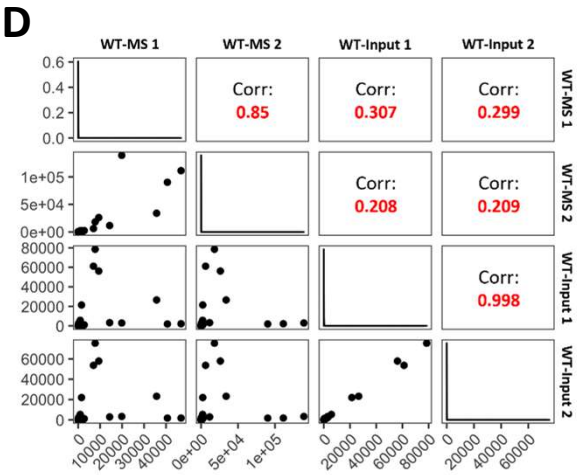

Correlations WT (Input vs MS)

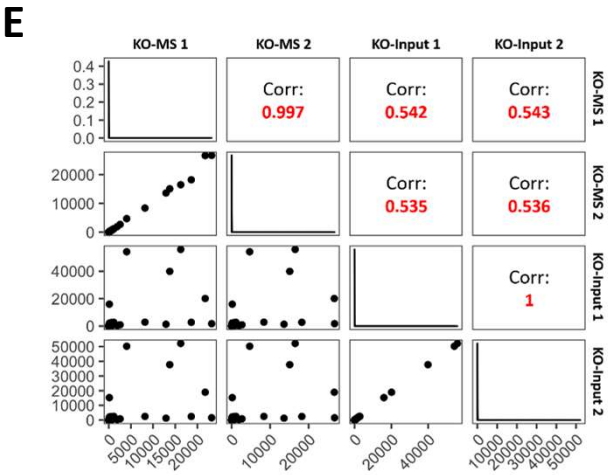

Correlations STAU1-KO (Input vs MS)

Figure S8. Validation of the reproducibility of RNA-Seq data. **A)** RNA-Seq data from replicates prepared from mitotic cell extracts (Input) and mitotic spindle preparations (MS) from WT and STAU1-KO (KO) cells were compared on PCA plot. **B-E)** High degree of correlation was observed between duplicates of cell extracts (Input) and of spindle preparations (MS), respectively, and weak correlation between Input vs MS preparations. Correlations between Input (A) and mitotic spindle replicates (B) in WT vs STAU1-KO HCT116 cells. Correlations between WT (C) and STAU1-KO (D) input vs MS.